JCB

Article

Cytotoxic granule endocytosis depends on the Flower protein

Hsin-Fang Chang,[1] Stefanie Mannebach,[2] Andreas Beck,[2,3] Keerthana Ravichandran,[1] Elmar Krause,[1] Katja Frohnweiler,[2] Claudia Fecher-Trost,[2] Claudia Schirra,[1] Varsha Pattu,[1] Veit Flockerzi,[2] and Jens Rettig[1]

[1]Cellular Neurophysiology, Center for Integrative Physiology and Molecular Medicine, [2]Department of Experimental and Clinical Pharmacology and Toxicology and Preclinical Center for Molecular Signaling, and [3]Center of Human and Molecular Biology, Saarland University, Homburg, Germany

Cytotoxic T lymphocytes (CTLs) kill target cells by the regulated release of cytotoxic substances from granules at the immunological synapse. To kill multiple target cells, CTLs use endocytosis of membrane components of cytotoxic granules. We studied the potential calcium dependence of endocytosis in mouse CTLs on Flower, which mediates the calcium dependence of synaptic vesicle endocytosis in *Drosophila melanogaster*. Flower is predominantly localized on intracellular vesicles that move to the synapse on target cell contact. Endocytosis is entirely blocked at an early stage in Flower-deficient CTLs and is rescued to wild-type level by reintroducing Flower or by raising extracellular calcium. A Flower mutant lacking binding sites for the endocytic adaptor AP-2 proteins fails to rescue endocytosis, indicating that Flower interacts with proteins of the endocytic machinery to mediate granule endocytosis. Thus, our data identify Flower as a key protein mediating granule endocytosis.

Introduction

Cytotoxic T lymphocytes (CTLs) are an important part of the adaptive immune system because they kill target cells by the release of cytotoxic substances from cytotoxic granules (CGs). Exocytosis of CGs is highly regulated and only occurs at a specialized target cell contact site, the immunological synapse (IS). It has been demonstrated early on that the process of IS formation, CG polarization, and probably also CG exocytosis is triggered by calcium (Lancki et al., 1987; Takayama and Sitkovsky, 1987; Leibson et al., 1990). Research over the past decades has revealed the molecular mechanism of this calcium signaling. First, the binding of T cell receptors to their ligand on the target cells triggers an intracellular signaling cascade that leads to the production of inositol 1,4,5-trisphosphate (IP_3). IP_3 binds to its receptor in the membrane of the ER, causing depletion of ER calcium stores and thus a raise in intracellular calcium. The loss of ER calcium is sensed by the ER membrane protein STIM1, which forms multimers, moves to the ER-plasma membrane apposition, and gates the opening of ORAI calcium channels in the plasma membrane (Hogan et al., 2010). Only this rise in intracellular calcium then leads to a plethora of cellular responses, from short-term reactions such as CG release to long-term reactions such as proliferation and cytokine production.

After exocytosis, CG membrane components are retrieved by endocytosis, a process highly important to ensure efficient serial killing of target cells (Griffiths et al., 2010). It has been shown recently in primary mouse CTLs that this process is distinct from regular endocytosis through recycling endosomes and depends on dynamin, clathrin, and the synaptobrevin2-specific adaptor protein CALM (Chang et al., 2016). Although it is well known that specific endocytosis of synaptic vesicles depends on calcium (Gad et al., 1998; Klingauf et al., 1998; Sankaranarayanan and Ryan, 2001), it is entirely unknown whether CG endocytosis at the IS of CTLs is calcium dependent and, if so, what molecular players are involved.

In *Drosophila melanogaster* it was shown that the calcium dependence of synaptic vesicle endocytosis depends on the vesicle-associated membrane protein Flower (Brose and Neher, 2009; Kuo and Trussell, 2009; Yao et al., 2009). However, these data were later challenged by Xue et al. (2012) who claimed that voltage-dependent calcium channels in the presynaptic plasma membrane were solely responsible for the calcium dependence of endocytosis. Furthermore, *Drosophila* Flower was later implicated in neuron survival (Rhiner et al., 2010; Merino et al., 2013; Pichaud, 2013; Gogna et al., 2015).

We show that the mouse homologue of Flower is present in CTLs, that it contains four transmembrane domains, and that it is localized predominantly to intracellular vesicles. To investigate its possible contribution to the endocytosis of CGs, we generated a Flower gene-deficient mouse. Absence of Flower alters neither the formation of IS nor the exocytosis of CGs at the IS. In contrast, endocytosis of CGs is entirely blocked at an early stage. Reintroduction of Flower or an increase in extracellular calcium can entirely rescue the Flower-mediated block of endocytosis, demonstrating an important

Correspondence to Jens Rettig: jrettig@uks.eu; Veit Flockerzi: Veit.Flockerzi@uks.eu

The Rockefeller University Press
J. Cell Biol. Vol. 217 No. 2 667–683
https://doi.org/10.1083/jcb.201706053

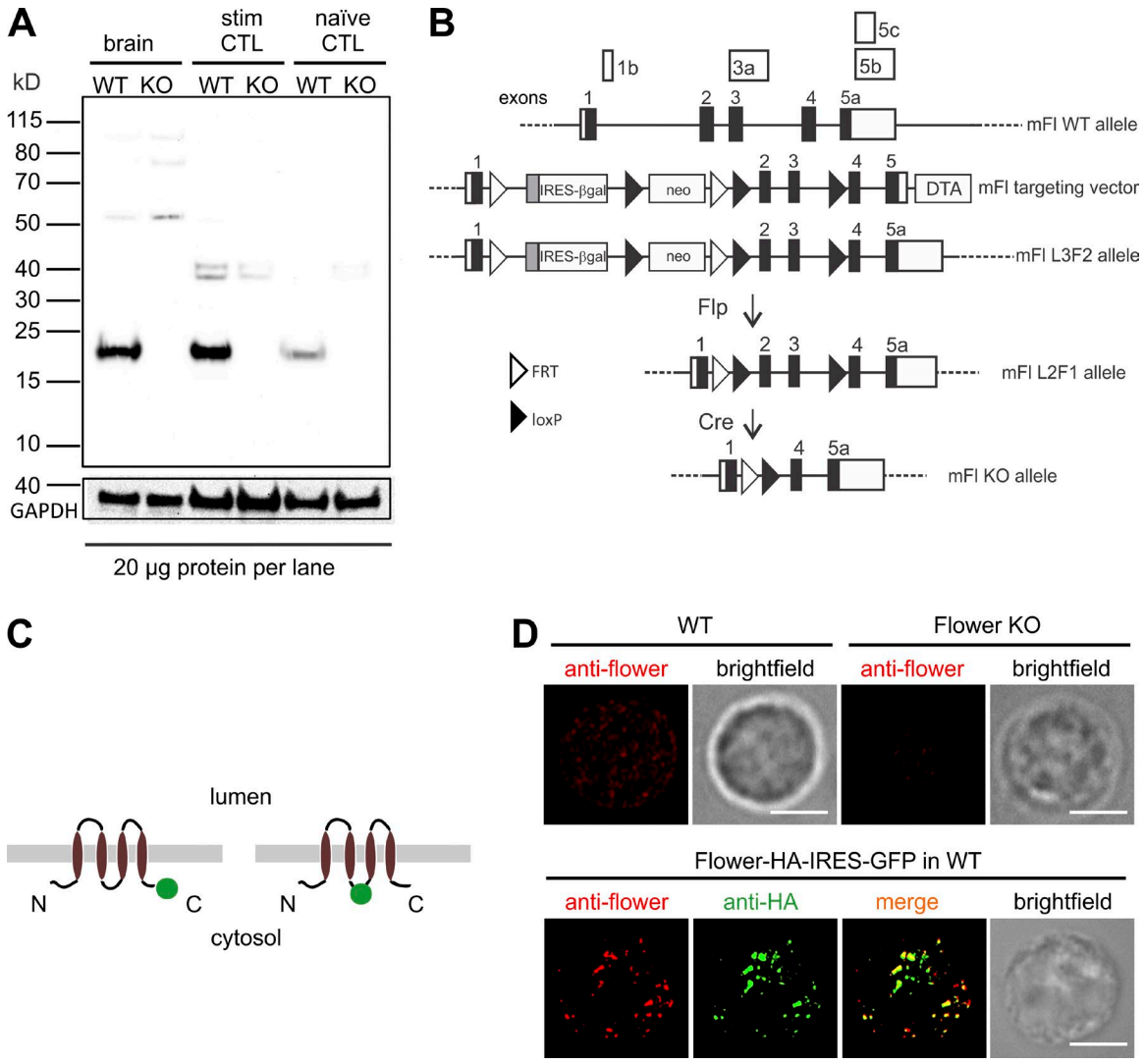

Figure 1. **Flower protein is expressed in primary CTLs from mouse. (A)** Western blot of lysates from whole-brain, stimulated (stim) CTLs and naive CTLs prepared from WT or Flower (*mFl*)-deficient mice (KO) by using the anti-Flower antibody and, to control protein loading, anti-GAPDH antibody. 20 µg total lysate was loaded per lane. The Flower protein is detected only in WT lysates at the expected molecular mass of ∼18 kD. **(B)** Generation of the $mFl^{-/-}$ mouse (see Fig. S2 for details). Scheme of the nontranslated (open boxes) and translated exons (closed boxes; not in scale, taken from Ensembl Genome Browser). WT *mFl* allele, targeting construct (HTGRS6009_A_G03; Eucomm), and recombinant mFl^{L3F2}, mFl^{L2F1}, and *mFl* KO alleles are shown. In the mFl^{L3F2} allele, exons 2 and 3 are flanked by lox P sites (closed triangles). An FRT (open triangles) sequence-flanked gene cassette comprises the SA-IRES-βGal followed by a promoter-driven neo cassette. Flp recombinase-mediated conversion of the L3F2 allele to the L2F1 allele and Cre recombinase-mediated conversion of the L2F1 to the KO allele (L1F1) are shown. DTA, diphtheria toxin A. **(C)** Cartoon showing the topology of Flower. The green circles indicate the position of the pHluorin fluorophore. N, N terminus; C, C terminus. **(D)** Localization of endogenous (top) and overexpressed (bottom) Flower-HA protein by using anti-Flower antibody in WT and Flower KO CTLs. Bars, 5 µm.

role for Flower in CTLs by facilitating endocytosis of CGs in a calcium-dependent manner.

Results

Flower protein is expressed in primary CTLs from mouse

Because Flower was initially discovered in *Drosophila* as a potential regulator of vesicle endocytosis at synapses, we focused our functional analysis on the IS formed between CTLs and target cells. At the IS, synapse formation, CG exocytosis, CG endocytosis, and synapse disassembly occur within 30 min, making this system ideal to study the molecular mechanism of regulated secretion.

First, we cloned the cDNA of the mouse homologue of Flower and generated an antibody against the recombinant full-length 171-aa protein (Fig. S1, A–C) to identify the protein in various tissues, including CTLs, by Western blot (Fig. 1 A and Fig. S1 D). Next, we deleted the mouse Flower gene by homologous recombination in embryonic stem cells (Fig. 1 B and Fig. S2) to generate homozygous Flower-deficient mice ($Fl^{-/-}$). These mice were viable, fertile, and showed no obvious phenotypic alterations in the cage environment. Breeding of heterozygous mice generated homozygous $Fl^{-/-}$ mice at the rate expected from the Mendelian frequency (Fig. S2).

The hydropathy profile of the 171 aa Flower predicts three to four transmembrane domains (Fig. S1 A). To obtain more detailed topological information, we fused the pH-sensitive fluorophore pHluorin to the C terminus of Flower or in between the

predicted second and third transmembrane domains (Fig. 1 C and Fig. S3). As a positive control, we used the CG membrane protein synaptobrevin2. After cDNA transfection in primary CTLs, we applied the protonophore carbonyl cyanide m-chlorophenyl hydrazone (CCCP), which leads to acidification of the cytoplasm. For both Flower constructs we observed a decrease in the fluorescence ratio on application of CCCP, indicating that these areas reside in the cytoplasm of CTLs (Fig. S3 A). To confirm these data, we fused mRFP to the C terminus of Flower from *Drosophila* and from mouse, transfected them into CTLs, and applied an Alexa Fluor 488–coupled anti-mRFP antibody to the extracellular bath solution. If Flower would have three transmembrane domains with its C terminus facing the extracellular space as proposed (Rhiner et al., 2010; Merino et al., 2013; Gogna et al., 2015), the antibody should bind to its epitope already in nonpermeabilized cells. As shown for the *Drosophila* Flower construct in Fig. S3 B, we observed no anti-mRFP488 signal in nonpermeabilized CTLs. In contrast, a clear signal was obtained after permeabilization, again arguing that the C terminus of Flower is located in the cytoplasm. Finally, we tested whether *Drosophila* and mouse Flower constructs colocalize in more differentiated cells, such as neurons, and found a nearly perfect colocalization (Fig. S3 C). From these experiments we conclude that Flower has four transmembrane domains (Fig. S3 A), that its N and C termini are located in the cytoplasm (Fig. 1 C and Fig. S3, A and B) and that this topology is conserved across species (Fig. S3, B and C).

The ∼18-kD Flower is readily detectable in Western blots with lysates from the brain and from naive and stimulated CTLs prepared from WT mice (Fig. 1 A). In comparison to 20 µg brain lysate as a positive control, we observed a band of similar intensity in 20 µg lysate from stimulated CTLs, whereas the expression level in naive CTLs was significantly lower (Fig. 1 A). No Flower protein was detectable in lysates from $FL^{-/-}$ mice, confirming the knockout (KO) and the specificity of the antibody.

To investigate the subcellular localization of Flower in primary CTLs, we fixed CTLs from WT and Flower-deficient mice and stained with the Flower antibody. Structured illumination microscopy (SIM) images revealed a weak, punctate signal in WT but not in Flower-deficient CTLs (Fig. 1 D, top). In addition, a small proportion of Flower appears to be located in the plasma membrane, which is confirmed by surface biotinylation of activated CTLs (Fig. S1 E). Expression of a Flower construct with a human influenza HA-tag confirmed the specificity of the anti-Flower antibody and the mostly punctate localization of Flower (Fig. 1 D, bottom). From these data we conclude that Flower is expressed in CTLs, that its expression is up-regulated on stimulation of CTLs, and that it is mostly localized to intracellular vesicles, generating a punctate expression pattern in immunocytochemistry.

Exocytosis of CGs and cellular calcium dynamics are unchanged in Flower-deficient CTLs

Because exocytosis and endocytosis of vesicles are tightly coupled to each other, we next wanted to rule out that the absence of Flower leads to any defects in exocytosis of CGs. For that purpose, we performed two independent experiments. First, we performed a degranulation assay that is widely used in immunology as the gold standard for the fusion of lysosomes and lysosome-related organelles like CGs by measuring the surface expression of LAMP1 (lysosome-associated membrane protein 1 or CD107a) by FACS. As shown in Fig. 2 A and quantified in Fig. 2 B, the degranulation of CTLs derived from WT and Flower-deficient mice were indistinguishable, with values of 57% and 55%, respectively, on stimulation (n = 10 and 5, respectively). As a second independent assay for CG exocytosis, we performed total internal reflection fluorescence microscopy (TIRFM) on CTLs derived from WT and Flower-deficient mice. CTLs were transfected with a synaptobrevin2-mRFP fusion construct to specifically label CGs (Matti et al., 2013). IS formation was induced by seeding the cells on CD3-coated coverslips, which ultimately resulted in the accumulation and exclusive fusion of CGs at the cell–glass interface (Pattu et al., 2011; Fig. 2 C). Quantification of TIRFM data revealed that neither the number of CTLs showing CG fusion (39.4 ± 5.3% for WT CTLs and 33.6 ± 4.4% for Flower-deficient CTLs; 104 WT and 119 Flower KO, n = 4; Fig. 2 D) nor the number of CG fusion events per cell (4.5 ± 0.8 for WT and 4.8 ± 0.9 for Flower KO; Fig. 2 E) were different between WT and Flower-deficient cells. We did observe, however, an increase in the latency of CG fusion in Flower-deficient CTLs compared with WT CTLs (117.3 ± 12.4 s for WT and 212.9 ± 17.7 s for Flower KO; Fig. 2 F). We observed a similar increase in the latency of the appearance of recycling endosomes, which fuse at the IS before CG arrival to deliver cargo essentially required for CG exocytosis (Marshall et al., 2015), in the TIRFM field (29.6 ± 9.5 s for WT, n = 7; 49.1 ± 8.9 s for Flower-deficient CTLs, n = 13; Fig. 2 G). To evaluate whether the absence of Flower has an effect on the global, cellular calcium dynamics of CTLs, we performed ratiometric fura measurements. CTLs from WT and Flower-deficient mice were incubated with 2 µM fura2-AM for 30 min and then plated on either p-ornithine–or anti-CD3–coated coverslips. As shown in Fig. 2 (H–M), both groups showed almost identical calcium dynamics under non-activating (p-ornithine) and activating (anti-CD3) conditions. In addition, raising the extracellular calcium concentration to 10 mM resulted in increased calcium signals with indistinguishable kinetics (Fig. 2 N). These data allow us to conclude that the absence of Flower has no influence on CG exocytosis and global calcium signaling of CTLs.

Lack of Flower leads to a complete block of CG endocytosis

Having shown that CG exocytosis is unchanged in the absence of Flower, we next tested whether there is any effect on CG endocytosis. Primary CTLs from WT and Flower-deficient mice were activated and transfected with synaptobrevin2-mRFP, a highly specific marker protein for CGs (Matti et al., 2013). We have previously shown that the fusion of mRFP to the C terminus does not interfere with the function of the protein but allows the use of an mRFP-specific antibody coupled to Alexa Fluor 488 to specifically visualize synaptobrevin2 upon fusion of CGs with the plasma membrane (Chang et al., 2016). Upon contact with target cells, real-time confocal microscopy of WT CTLs showed a clear accumulation of CGs (indicated by the mRFP fluorescence) at the contact zone, the IS (Fig. 3 A, top, time 0'00"). Because the Alexa Fluor 488–coupled anti-mRFP antibody (anti-RFP488) was present in the medium throughout the experiment, yellow puncta started to appear in images at later time points, indicating fusion of CGs. Over time, endocytosis of CGs and their membrane proteins was observed as the puncta moved away from the IS (Fig. 3 A and Video 1). We quantified the effectiveness of endocytosis by analyzing the fluorescence

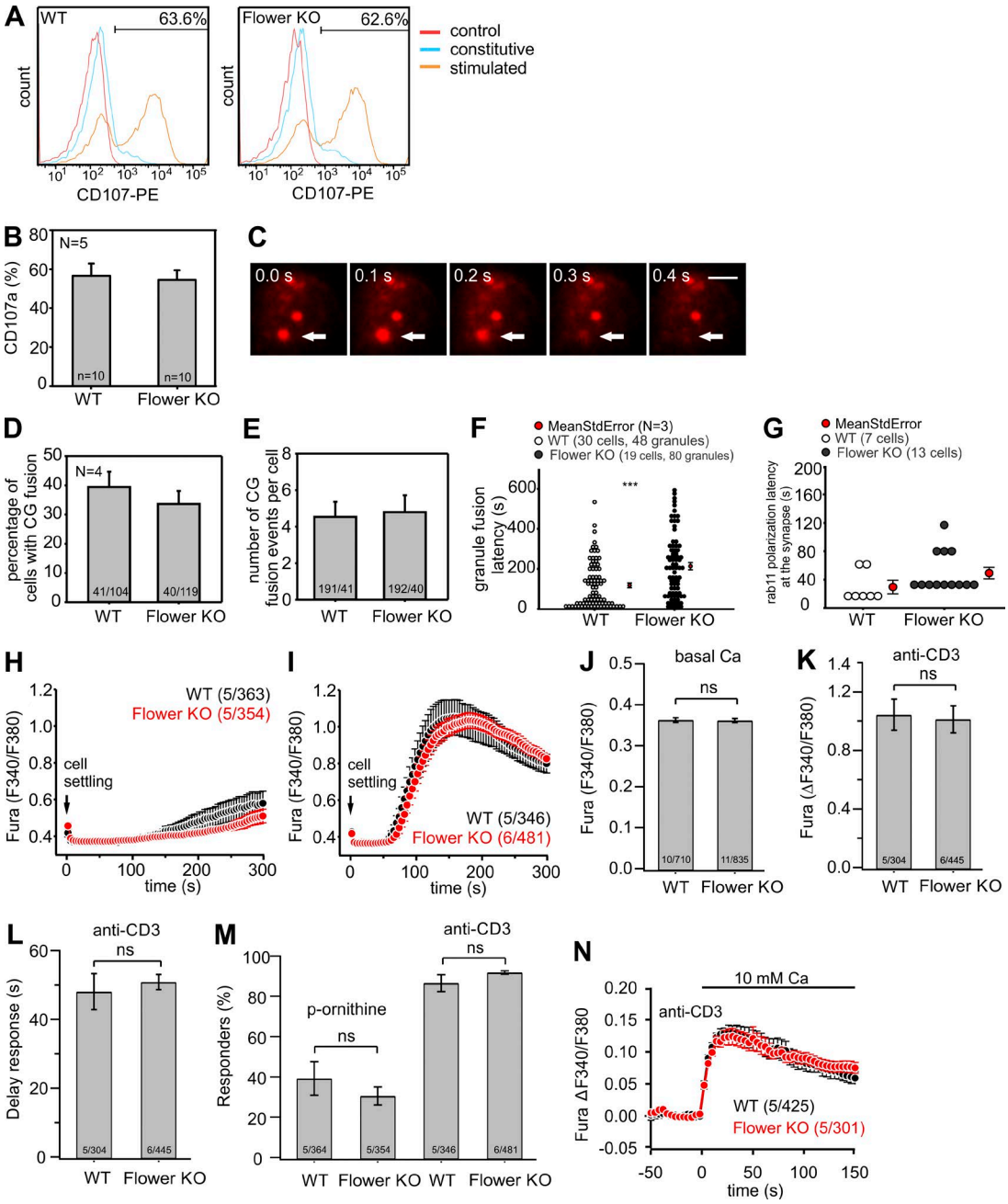

Figure 2. **Exocytosis of CGs is unchanged in Flower-deficient CTLs. (A)** FACS-based degranulation assay with CTLs derived from WT and Flower-deficient mice by using CD107-PE conjugated antibody. Cells were stimulated with 10 µg anti-CD3 antibody and compared with unstimulated (constitutive) cells. Cells in the absence of CD107-PE antibody served as controls. One representative experiment of five (see B) is shown. **(B)** Statistical analysis of the average percentage of cells exhibiting CD107a fluorescence at the plasma membrane after stimulation ($N = 5$; $n = 10$). **(C)** Representative TIRFM serial images showing the fusion of a CG (arrow). Bar, 2 µm. **(D and E)** CG fusion analysis. CTLs from WT and Flower-deficient mice were transfected with syb2-mRFP as a CG marker. Cells were plated on anti-CD3–coated coverslips and perfused with 1 mM calcium buffer for TIRFM recording. Percentage of cells that show CG fusion (D) and the number of fusion events per cell (E) are shown. **(F)** CG fusion latency. CTLs were transfected with syb2-mRFP as a CG marker. CG fusion events were triggered by seeding CTLs on anti-CD3 antibody-coated glass coverslips. The fusion latency expresses the duration from the first granule appearing in the TIRFM plane to the fusion of individual CGs. Unpaired Student's *t* test: ***, $P < 0.001$. **(G)** Polarization latency of recycling endosomes (REs). CTLs were transfected with rab11-mCherry as an RE marker and recorded in 1 mM calcium buffer by TIRFM. The polarization latency of the duration from a CTL attaching to the anti-CD3 coated coverslip to the first RE appearing in the TIRFM plane. **(H and I)** Ratiometric imaging of cytosolic calcium (Fura F340/F380) in CTLs derived from WT (black) and Flower-deficient (red) mice seeded on poly-L-ornithine (H)– and anti-CD3 (I)–coated coverslips. **(J–M)** Quantification of data shown in panels H and I. Basic cytosolic calcium levels (Fura F340/F380) (J), amplitude of the anti-CD3–mediated cytosolic calcium increase (K), delay of the calcium increase (L), as well as the percentage of cells responding with an increase of cytosolic calcium while seeded on poly-L-ornithine and anti-CD3–coated coverslips (M) were not significantly different in CTLs derived from WT and Flower-deficient mice. **(N)** Ratiometric imaging of cytosolic calcium (Fura F340/F380) in CTLs derived from WT (black) and Flower-deficient (red) mice seeded on anti-CD3–coated coverslips after the addition of 10 mM extracellular calcium. Data in B, D, E, and H–N are given as mean ± SEM, and the number of experiments (x) and cells (n) is shown in brackets (x/n). Two-tailed unpaired Student's *t* tests were performed.

intensity of anti-RFP488 at the IS versus that of the entire CTL (see Materials and methods for details; Chang et al., 2016). Starting from 100% at the time of contact, the fluorescence in WT CTLs gradually decreased to 33.3 ± 3.1% (n = 20) after 15 min (Fig. 3 B, closed circles). Because this value is close to the expected percentage of a random distribution (28.9%), we can conclude that CG endocytosis in WT CTLs is completed within 15 min after target cell contact. In contrast, CTLs from Flower-deficient mice showed virtually no decline of fluorescence over the 15-min recording period, indicating a complete block of CG endocytosis (96.3 ± 1.4%; n = 20; P < 0.001; Fig. 3, A [middle] and B [open circles]; and Video 1). A 3D reconstruction shown in Video 2 clearly demonstrates the block of CG endocytosis in the absence of Flower. This block is exclusively to the result of the absence of Flower, because reintroduction of a Flower-pHluorin construct into Flower-deficient CTLs completely rescued endocytosis back to WT levels (38.0 ± 7.5%; n = 20; P < 0.001; Fig. 3, A [bottom] and B [closed triangles]). To confirm that the observed effect is not contaminated by the overexpression of synaptobrevin2-mRFP, we crossed the Flower-deficient mouse line with our recently described synaptobrevin2-mRFP knock-in (SybKI) mouse in which the endogenous synaptobrevin2 was replaced by a synaptobrevin2-mRFP fusion protein. Because the Syb2-mRFP remained under the control of the endogenous synaptobrevin2 promotor, every expressed synaptobrevin2 molecule in CTLs was labeled by the mRFP fluorophore (Matti et al., 2013). We observed the same block of endocytosis in Flower KO/SybKI CTLs as in WT CTLs overexpressing synaptobrevin2-mRFP, whereas endocytosis was unaffected in SybKI CTLs (Fig. 3 C). Moreover, expression of Flower-pHluorin in Flower KO/SybKI CTLs rescued endocytosis as efficiently as in WT CTLs overexpressing synaptobrevin2-mRFP (compare anti-RFP647 fluorescence of the top CTL in Fig. 3 D expressing Flower-pHluorin with that of the lower CTL not expressing Flower-pHluorin). These data demonstrate that the absence of Flower leads to a complete block of CG endocytosis. Because we have previously shown that the block of CG endocytosis leads to a reduction in serial killing capability of CTLs (Chang et al., 2016), we performed a population-based killing assay with WT and Flower-deficient CTLs using different effector/target cell ratios (Fig. 3, E and F). As predicted, Flower-deficient CTLs showed a reduced killing capability that was most pronounced at low effector/target cell ratios. Therefore, we conclude that the absence of Flower and the resulting block of CG endocytosis has significant consequences for the main function of CTLs, the serial killing of target cells.

Flower deficiency blocks an early step of CG endocytosis

We next wanted to investigate at which step the endocytosis of CG is blocked. For that purpose, we performed correlative light and electron microscopy (CLEM) on Flower KO/SybKI CTLs that had been in contact with target cells in the presence of anti-RFP488 antibody in the medium. As shown in Fig. 4 A (bottom), the entire fluorescence of the anti-RFP488 antibody was detected at the interfaces between CTL and target cells, the IS. In contrast, fully endocytosed vesicles could be readily observed in control SybKI CTLs (Fig. 4 A, top). Further magnification revealed that endocytic necks, which are typical for dynamin-mediated, late-fission events, were lacking in Flower-deficient CTLs. Rather, a flat membrane thickening with pit-like structures was observed (Fig. 4, B and C, bottom). We quantified the distribution of 147 and 136 fluorescent signals in Flower KO/SybKI and SybKI control CTLs, respectively. In accordance with the confocal data shown in Fig. 3, Flower-deficient CTLs showed a higher percentage of fluorescent puncta at the IS compared with control CTLs (Fig. 4 D). Conversely, the percentage of fluorescent puncta away from the IS was significantly larger in control cells compared with Flower-deficient cells (P < 0.01). Furthermore, Flower-deficient cells showed a significantly higher number of pit-like structures at the IS compared with control CTLs (Fig. 4 E; P < 0.01). Thus, our CLEM analysis revealed that the absence of Flower blocks CG endocytosis at a very early stage, even before membrane budding occurs.

Increased calcium concentration rescues the Flower deficiency-mediated block of CG endocytosis

In neurons it is established that the endocytosis of synaptic vesicles is dependent on the intracellular calcium concentration (Gad et al., 1998; Klingauf et al., 1998; Sankaranarayanan and Ryan, 2001). Because Flower had been shown to have some sequence similarity to calcium and transient receptor potential channels (Yao et al., 2009), we speculated that Flower might be involved in the calcium signaling initiating endocytosis. We therefore tested whether the provision of calcium through other sources might rescue the block of CG endocytosis in Flower-deficient CTLs. We again performed real-time confocal microscopy of WT and Flower-deficient CTLs in the presence of anti-RFP488 antibody in the medium and observed normal CG endocytosis in WT CTLs (57.4 ± 5.9% after 7.5 min; n = 22) and a complete block of endocytosis in Flower-deficient CTLs (96.9 ± 1.4% after 7.5 min; n = 23; Fig. 5, A and B; and Video 3). After 7.5 min 10 mM calcium was added to the bath solution. The increase in the driving force for calcium influx resulted in a decrease in the fluorescence decay at the IS in WT CTLs, which is caused by additional exocytosis of CGs. Interestingly, Flower-deficient CTLs responded to the increase in extracellular calcium almost instantly by starting to endocytose CGs, which was already detectable 30 s after the addition of 10 mM calcium (Fig. 5 A, bottom, time point 8'00"; and Video 3). After 15 min the fluorescence at the IS decreased to 27.4 ± 5.8% (n = 23), indicating that CG endocytosis was fully rescued back to WT levels (Fig. 3, compare A and B). These data show that the presence of Flower is required for the efficient endocytosis of CGs and that the block of endocytosis caused by the lack of Flower can be overcome by providing calcium through other sources.

Flower is localized on intracellular vesicles

So far, our data showed a requirement for Flower for efficient CG endocytosis at the IS and an involvement of Flower in the calcium signaling initiating this event. To learn more about the mechanism of CG endocytosis, we next asked where Flower is localized in CTLs. It is evident from Fig. 1 that both endogenous and overexpressed Flower have a mostly punctate expression pattern in CTLs, indicating a localization on intracellular vesicles. To test whether these intracellular vesicles represent endosomal compartments, we transfected mCherry fusion constructs of rab5 (early endosome marker), rab7 (late endosome marker), and rab11 (recycling endosome marker) in WT CTLs and stained these cells after fixation with the anti-Flower antibody. Although all endosomal markers showed the expected punctate staining (Fig. 6 A), quantification of potential co-

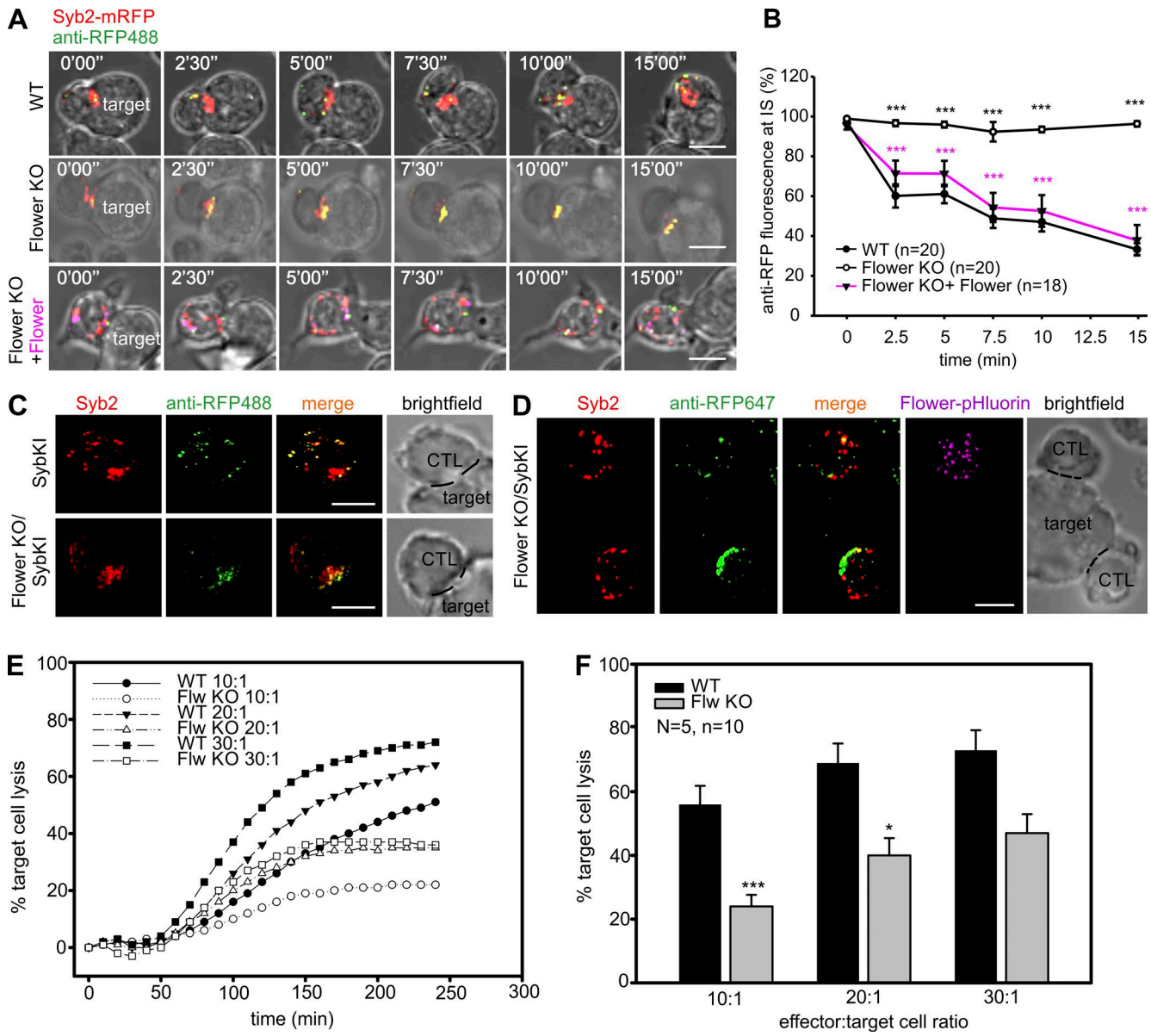

Figure 3. **CTLs from Flower-deficient mice show a specific block of CG endocytosis. (A)** Time-lapse maximal-intensity projections of syb2-mRFP (red) transfected CTLs conjugated to target cells in the presence of anti-RFP488 antibody (green) in the medium. The endocytosis of CGs (yellow) is shown in WT (top), Flower-deficient (middle), and Flower-deficient CTLs overexpressing Flower-pHluorin (magenta; bottom). Bars, 10 µm. **(B)** Quantitative analysis of the accumulation of endocytic CGs at the IS (one third of CTL volume projecting toward the target cell) over time from panel A. Time zero is defined as the appearance of the first endocytic CG at the IS. Data are given as mean ± SEM; unpaired Student's *t* test: ***, $P < 0.001$. **(C)** CTLs from synaptobrevin2-mRFP knock-in (SybKI; top) and Flower-deficient/SybKI (Flower KO/SybKI; bottom) mice were incubated with target cells (P815) in the presence of Alexa Fluor 488–conjugated anti-RFP antibody (anti-RFP488) in the medium to visualize endocytic granules. Cells were then fixed after 40 min and imaged by SIM. Bars, 5 µm. **(D)** CTLs from Flower KO/SybKI (bottom) mice were electroporated with Flower-pHluorin and incubated with target cells (P815) in the presence of Alexa Fluor 647–conjugated anti-RFP antibody (anti-RFP647) in the medium to visualize endocytic granules. Cells were then fixed after 40 min and imaged by SIM. The CTL expressing Flower-pHluorin (top cell) shows a clear rescue in endocytosis, whereas the untransfected one (bottom cell) does not. Bar, 5 µm. **(E and F)** Real-time calcein release-based killing assay. WT and Flower-deficient CTLs were co-cultured with P815 cells at the indicated CTL/target cell ratios, and killing was measured every 10 min for 4 h. Data are given as mean ± SEM from five independent experiments performed in duplicates ($n = 10$; $N = 5$). One-tailed unpaired Student's *t* test: *, $P < 0.05$; ***, $P < 0.001$.

localization by Manders' overlap coefficient (Manders et al., 1993) revealed basically no overlap between the individual endosome compartments and Flower (Fig. 6 B). We also tested for a potential localization of Flower on CGs by staining CTLs derived from SybKI mice with the anti-Flower antibody and by costaining WT CTLs with anti-granzyme B and anti-Flower antibodies (Fig. 6 A). Again, Manders' overlap coefficient revealed no overlap between synaptobrevin2 and Flower or GzmB and Flower fluorescence (Fig. 6 B), ruling out that Flower is localized on CGs.

Assuming that Flower is localized in yet-to-be identified intracellular compartments/vesicles, we next tested how these Flower-containing vesicles would behave on target cell contact of CTLs. For that purpose, we cotransfected Flower-deficient CTLs with syb2-mRFP to label CGs and Flower-pHluorin to label Flower-containing vesicles. 12 h after transfection, target

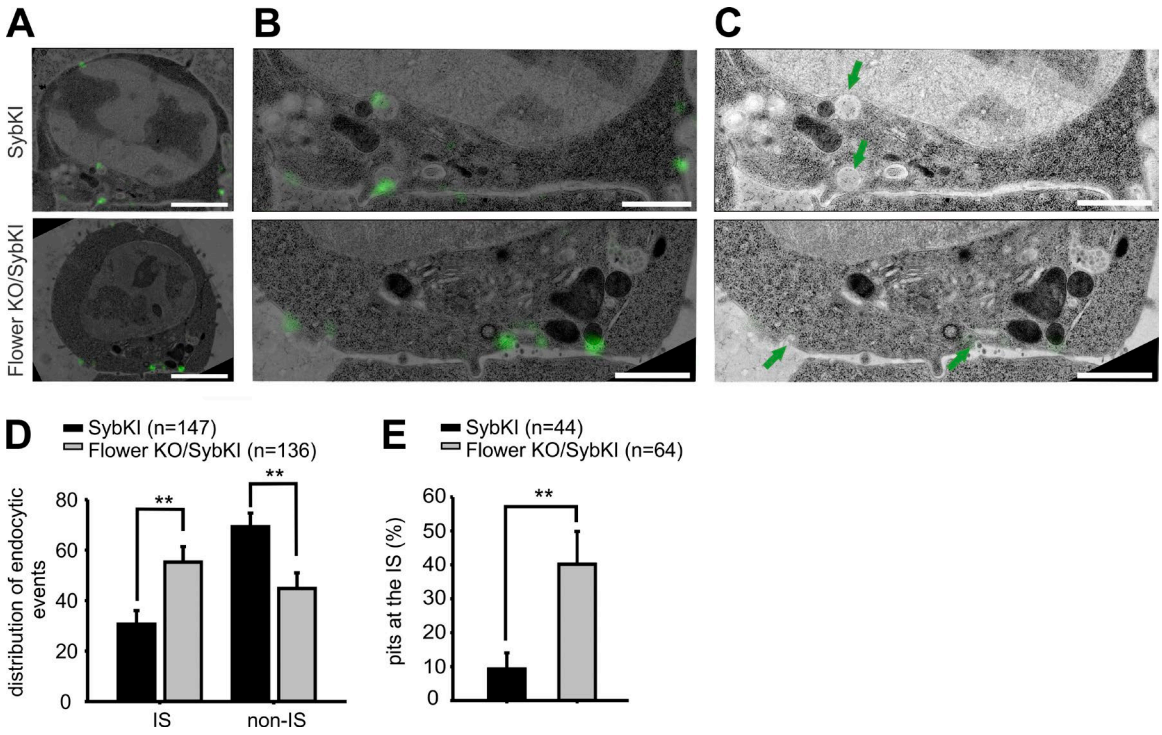

Figure 4. **CG endocytosis is blocked at an early stage in Flower-deficient CTLs. (A)** CLEM composite images of SybKI CTL (top) and Flower KO/SybKI CTL (bottom) in contact with the target cell. CTLs were incubated with target cells for 35 min in the presence of anti-RFP488 (green) in the medium to label endocytic CGs. After fixation, the processed fluorescent SIM image was overlaid with the transmission electron microscopy (TEM) image. Bars, 2 µm. **(B)** Magnification images from panel A of CTL and target cell contact region. Bars, 2 µm. **(C)** TEM images with green arrows marked the endocytic events in the SIM images. Bars, 1 µm. **(D)** Quantitative analysis of endocytic events distribution in SybKI CTLs (control) and Flower KO/SybKI CTLs from the CLEM experiment. The IS is defined as the interface between the CTL and target cells at the contacted membrane. The non-IS region is the remaining part in CTLs including cytoplasm and plasma membrane aside contact site. 147 endocytic events were analyzed from SybKI CTLs (n = 25), and 136 endocytic events were analyzed from Flower KO/SybKI CTLs (n = 26). **(E)** Quantitative analysis of ultrastructure of endocytic events at the IS corresponding to anti-RFP488 fluorescence green spots. Relative frequency of pit-like structures over total events were shown in the graph from SybKI CTLs (n = 25) and Flower KO/SybKI CTLs (n = 26). Data are given as mean ± SEM; Mann–Whitney U test; **, $P < 0.01$.

cells were added in the presence of Alexa Fluor 405–labeled anti-RFP antibody (anti-RFP405) in the medium, and time-lapse confocal microscopy was performed (Fig. 7 A and Video 4). Immediately after contacting the target cells, Flower-containing vesicles moved toward the IS where they stayed until the end of the 20-min recording period. Endocytosis of CGs, indicated by the appearance of the anti-RFP405 fluorescence, was first observed ∼8 min after initial contact (Fig. 7 A, top panel of the snapshot at 7'51"). The fluorescence of the endocytosing granules was adjacent to the fluorescence of the Flower-containing vesicles, indicating that they were in close apposition but not colocalizing (Fig. 7 A). We also tested whether there was a temporal segregation between the appearance of CGs and Flower-containing vesicles at the IS. As shown in the bottom panels of Fig. 7 A, no apparent difference was detectable with the temporal and spatial resolution provided by confocal microscopy. To improve both temporal and spatial resolution, we performed TIRFM on CTLs transfected with syb2-mRFP and Flower-pHluorin (Fig. 7 B). Our TIRFM setup provides a z-resolution of ∼180 nm and an acquisition frequency of 10 Hz. CTLs were plated on anti-CD3–coated coverslips, and the appearance of both classes of vesicles was imaged for 50 s (Fig. 7 B and Video 5). Quantification of the number of vesicles over time showed that the average number of Flower-containing vesicles was larger than the number of CGs during the entire recording period (Fig. 7 C). Moreover, Flower-containing vesicles started to appear almost immediately after plating, whereas CGs appeared with a delay of ∼30 s. These data support our finding that Flower is not localized on CGs and demonstrate that Flower-containing vesicles arrive at the IS before CGs.

A Flower mutant defective in endocytosis does not rescue the Flower deficiency-mediated block of CG endocytosis

A key step in endocytosis is the binding of the adaptor protein AP-2 to membrane proteins that are to be endocytosed (Mahaffey et al., 1990; Matsui and Kirchhausen, 1990; Beck and Keen, 1991). We identified two putative AP-2 binding motifs (YXXΦ) on Flower immediately before the first and immediately after the last transmembrane domain (Fig. 8 A). For testing assembly of Flower and AP complexes, we performed antibody-based affinity purifications of Flower-containing protein complexes from solubilized brain proteins and from CTL lysates followed by mass spectrometry (MS). The antibodies used were the anti-Flower antibody (Fig. S1) and, as a control, nonspecific immunoglobulins. This approach robustly identified the Flower protein (Fig. S4 and Table S1). In addition, components of the AP complexes were clearly identified in the anti-Flower eluates, arguing that this interaction indeed occurs in vivo (Fig. S4, A–D; and Table S1). The amount of AP-2 complexes associated with the mutant Flower protein, obtained by replacing the amino acid residues of both AP-2 binding motifs by alanine residues (Fig. 8 A) was reduced by ≥62% compared with the amount of AP-2 complexes associated with the WT Flower protein (Fig.

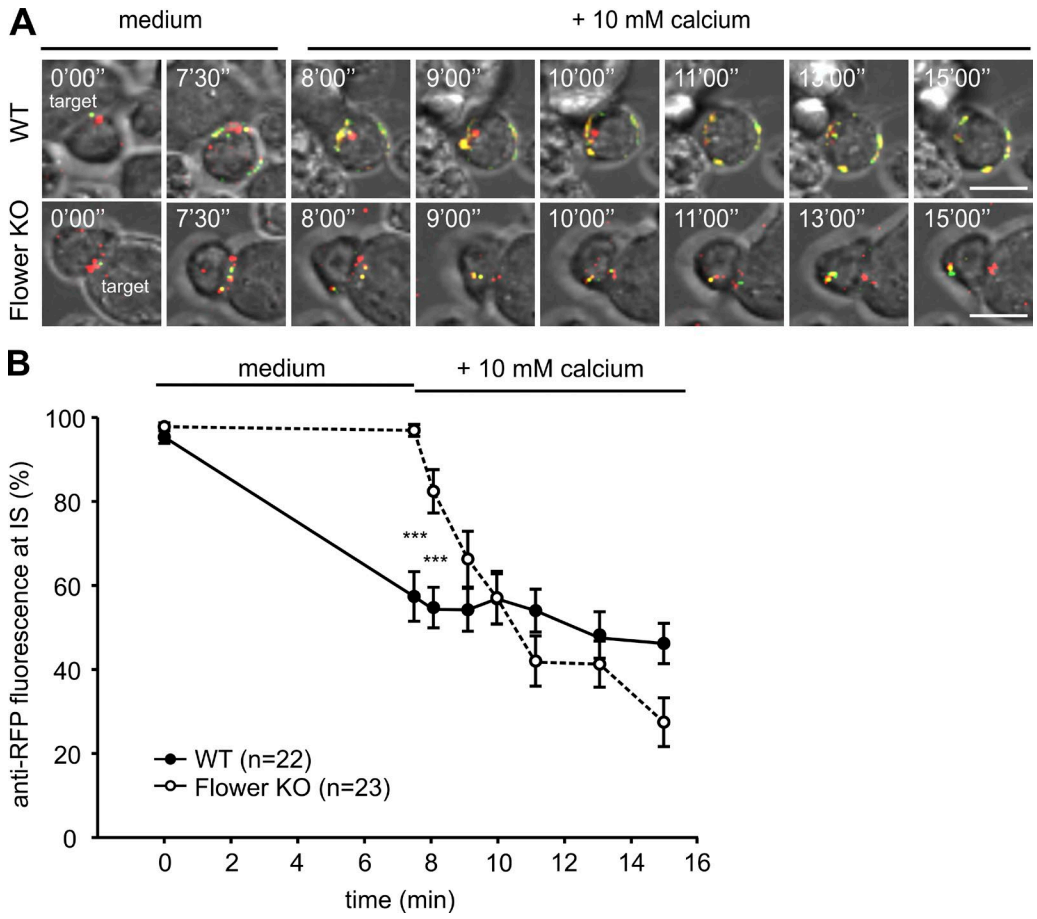

Figure 5. **Elevation of extracellular calcium rescues the endocytosis defect in Flower-deficient CTLs. (A)** Time-lapse maximal-intensity projections of syb2-mRFP (red) transfected CTLs in contact with target cells before and after application of extracellular buffer containing 10 mM calcium. CTLs were incubated with target cells in the presence of anti-RFP488 antibody (green) in the medium for 30 min and then perfused with 10 mM calcium buffer. Bars, 10 µm. **(B)** Quantitative analysis of the accumulation of endocytic CGs at the IS (one third of CTL volume projecting toward the target cell) over time from panel A. Time zero is defined as the appearance of the first endocytic CG at the IS. Data are given as mean ± SEM; unpaired Student's *t* test: ***, P < 0.001.

S4 E), confirming that interaction of AP2-complexes with the Flower mutant was disturbed. Expression of the Flower mutant cDNA resulted, in comparison to the preferential vesicular localization of WT Flower, in a predominantly plasma membrane localization of Flower (Fig. 8, B and C), indicating that these recognition sites are involved in the endocytosis of Flower.

We then asked whether the altered localization of the mutant would affect the ability to rescue the endocytosis defect in Flower-deficient cells. As shown in Fig. 8 D and quantified in Fig. 8 E, reintroduction of the Flower mutant did not, in stark contrast to WT Flower, rescue the endocytosis defect of Flower-deficient CTLs. We conclude from these data that Flower either exerts its effect while being localized on intracellular vesicles or that exocytosis of Flower is a prerequisite for its function in endocytosis (see Discussion).

Discussion

We here identify the Flower protein as an instrumental part of the calcium-dependent endocytosis of CGs in primary T lymphocytes. The absence of Flower leads to a time-dependent block of endocytosis at an early stage that can be rescued by the reintroduction of Flower or by raising the extracellular calcium concentration. High-resolution fluorescence revealed that Flower is mostly located on intracellular vesicles, with a minor fraction located in the plasma membrane.

Flower was originally identified in *Drosophila* in an unbiased genetic forward screen for mutants affecting synaptic transmission (Yao et al., 2009). Flower mutants are lethal and lead to a vast enlargement of presynaptic area of the neuromuscular junction, indicating a defect in endocytic retrieval. In the *Drosophila* neuromuscular junction, Flower is localized to two areas, the synaptic vesicle membrane and the presynaptic plasma membrane. Its proposed topology of four transmembrane domains and the resemblance of a part of its sequence to the selectivity filter of calcium and transient receptor potential channels led to the hypothesis that Flower acts, -on fusion of synaptic vesicles with the plasma membrane, as a calcium channel to specifically trigger endocytosis (Yao et al., 2009), although supporting evidence was scarce (Brose and Neher, 2009). Xue et al. (2012) later showed by patch-clamp measurements in the Calyx of Held synapse that the addition of synaptic vesicle membrane into the plasma membrane does not lead to an additional calcium current.

In this paper, we give evidence that Flower comprises four transmembrane domains (Fig. S3) and is localized on intracellular vesicles and, to a minor extent, on the plasma membrane

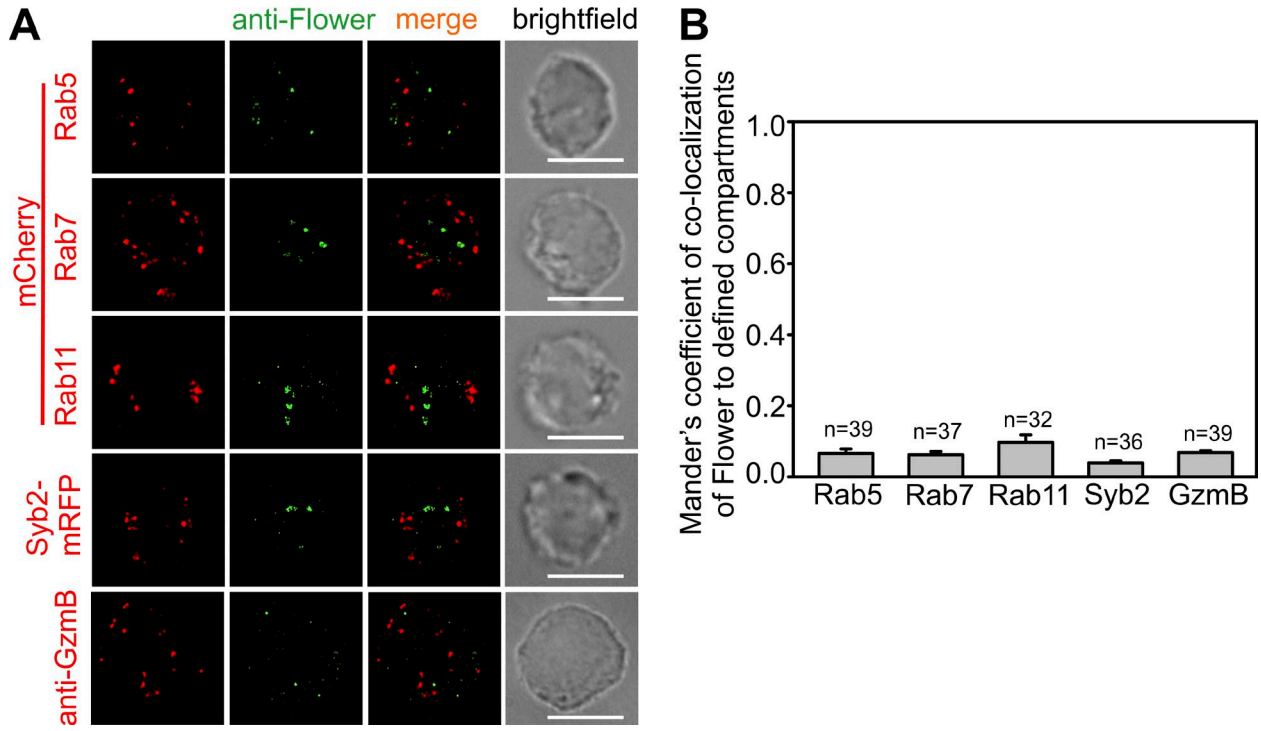

Figure 6. **Flower is localized on intracellular vesicles but not on CGs or on endosomal compartments. (A)** SIM images of anti-Flower antibody staining (green) on stimulated WT CTLs transfected with different endosome markers (red, mCherry), CTLs with endogenously labeled CGs from SybKI mice (SybKI CTLs), and WT CTLs costained with anti-GzmB antibody. Bars, 5 µm. **(B)** Manders' overlap coefficient of anti-Flower to rab5-, rab7-, rab11-, or syb2-positive compartments. Data are given as mean ± SEM.

(Figs. 1, 6, 7, 8, and S3). In contrast to what has been described in neurons (Yao et al., 2009), we find that these intracellular vesicles do not correspond to the vesicles secreted at the synapse (i.e., CG), but also do not contain markers for early, late, and recycling endosomes (Fig. 6). The apparent lack of identity of these vesicles in conjunction with the fact that their fusion in TIRFM experiments on IS formation was not detectable (unpublished data) might explain why electrophysiological recordings did not yield any calcium currents (Xue et al., 2012, and results from this study). Still, the fact that extracellular calcium could rescue the block of endocytosis in Flower-deficient cells indicates that Flower exerts its function through calcium signaling, although alternative possibilities still exist (Yao et al., 2017). One possible scenario is depicted in Fig. 9 A, in which Flower would release calcium from the lumen of these intracellular vesicles to generate a calcium microdomain underneath the plasma membrane that would be sufficient to trigger endocytosis of this plasma membrane patch. Although this scenario would be in accordance with data in other studies (Yao et al., 2009; Xue et al., 2012), it is very challenging to prove. Not only are putative ion channels on intracellular Flower-containing vesicles hardly accessible to patch-clamp experiments because of the small surface area of those vesicles, calcium measurements with selective indicators are also difficult. As pointed out, we currently do not know the composition of Flower-containing vesicles. Therefore, we cannot attach an appropriate calcium indicator, such as GCaMP, to either a resident protein or a specific localization signal. Attempts to fuse GCaMP to one of the intraluminal loops or to single transmembrane domains of Flower have resulted in a mislocalization of the fusion proteins (unpublished data), apparently because of the small size of the loops (approximately two to four amino acid residues) or the truncated proteins.

An alternative scenario to explain Flower function in endocytosis is depicted in Fig. 9 B. Although we did not observe fusion of Flower-containing vesicles on IS formation and during CG fusion, Flower clearly is located partially in the plasma membrane (Fig. 8 B). Thus, it remains possible that Flower exerts its function while being integrated into the plasma membrane, as originally postulated by Yao et al. (2009). One might speculate that once in the plasma membrane Flower mediates calcium influx from the extracellular space. However, in agreement with Xue et al. (2012) and a recent publication from Yao et al. (2017), we were unable to measure an increase in cytoplasmic calcium in primary CTLs on expression of Flower (unpublished data). Moreover, even the expression of the Flower mutant, which in contrast to WT Flower has a significant plasma membrane localization, did not induce increased cytoplasmic calcium concentrations. Thus, although we cannot rule out the possibility that the correct trigger for induction of Flower-mediated calcium transients has not yet been identified, we consider the function of Flower as a calcium channel in the plasma membrane unlikely. This notion is strengthened by a recent study demonstrating that Flower regulates clathrin-mediated endocytosis in a calcium-independent manner (Yao et al., 2017). Instead, Flower in the plasma membrane might serve as a recruitment platform for AP-2, thereby increasing the concentration of AP-2 and clathrin to a value sufficient to trigger endocytosis of membrane patches. These endocytosis "hot spots" clearly exist, because we regularly found an accumulation of anti-RFP fluorescence at the IS for prolonged periods of time on different manipulations that block endocytosis (dynasore, pitstop, and CALM siRNA in the study by Chang et al. [2016]; Flower KO in this study). Our finding that the Flower mutant is unable to rescue the endocytosis defect in Flower-deficient CTLs (Fig. 8) is fully compatible

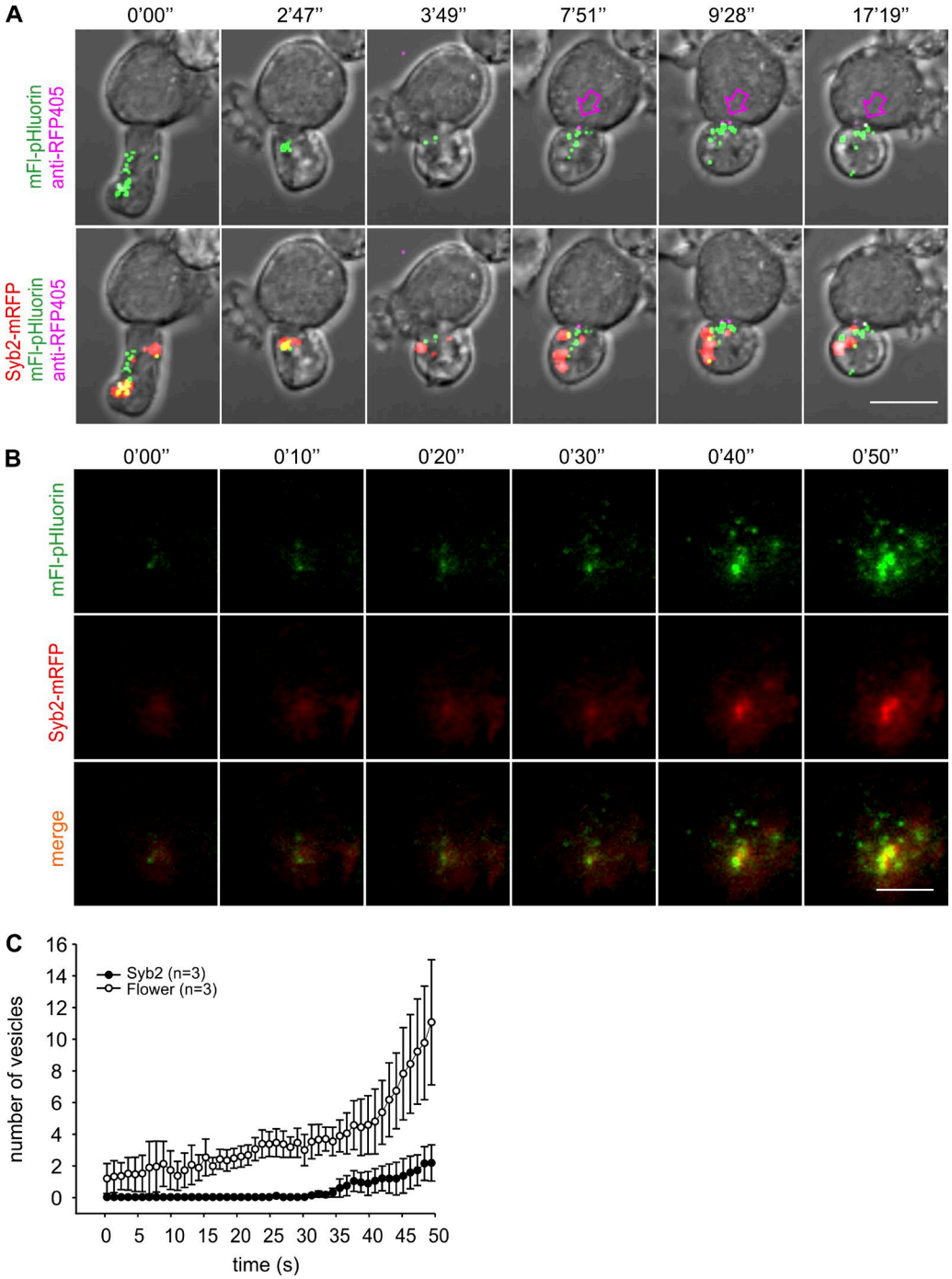

Figure 7. **Flower-containing vesicles are polarized earlier to the IS than to CGs and localize around endocytic CGs. (A)** Time-lapse maximal-intensity projections of a Flower-deficient CTL transfected with Flower-pHluorin (green) and syb2-mRFP (red) and conjugated to a target cell in the presence of anti-RFP405 antibody in the medium. The arrows point to the endocytic CGs (magenta). Bar, 10 µm. **(B)** Real-time dynamics of Flower-containing vesicles and CGs in CTL monitored by TIRFM. Flower-deficient CTLs were transfected with Flower-pHluorin (green) and syb2-mRFP (red). Bar, 5 µm. **(C)** Quantitative analysis from panel B of the number of vesicles arriving at the IS over time. Data are given as mean ± SEM.

with this alternative scenario. Clearly, more experiments are required to be able to distinguish between the two possibilities.

Materials and methods

Reagents and antibodies

Protein transport inhibitor, Golgi-stop, was purchased from BD Biosciences. CCCP and poly-ornithine were purchased from Sigma. All plasmids and antibodies generated and used in the laboratories of the authors are listed in Tables S2 and S3.

Generation of antibodies for mouse Flower

The cDNA of calcium channel flower domain-containing protein 1 (Cacfd1, synonym calcium channel flower homologue or Flower) was cloned from mouse brain and sequenced on both strands (Fig. S1). The full-length 516 nucleotide cDNA (NM_029862) was expressed as a His6-Sumo-mFl fusion protein in *Escherichia coli* Rosetta (DE3)-

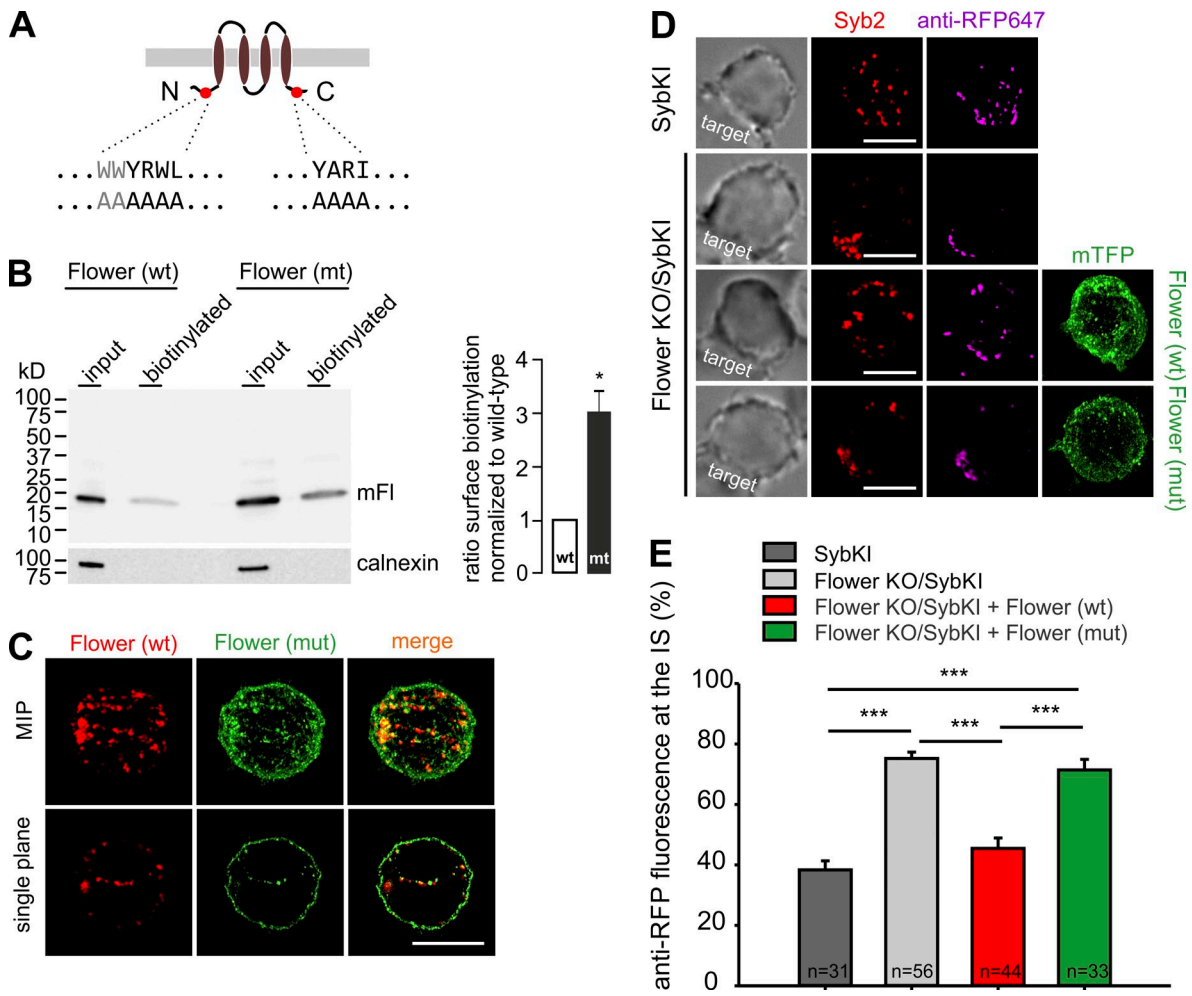

Figure 8. **Flower mutant cannot rescue the endocytosis defect. (A)** Positions of the putative AP-2–binding motifs within Flower (red circles) with the WT and mutated sequences below. N, N terminus; C, C terminus. **(B)** Western blot (left panel, 4 to 20% SDS polyacrylamide gel) of surface-expressed Flower WT and mutant (mut) cDNAs in Cos-7 cells were detected by the Flower antibody. The ER protein calnexin was used as the control. One representative of six experiments that indicate more than threefold higher plasma membrane expression of the mutant protein compared with the WT protein (right; mean ± SEM; $n = 6$; **, $P < 0.005$, one sample t test). **(C)** SIM images (maximal-intensity projections [MIP] and single planes through the middle of the cell) of a CTL cotransfected with WT tagRFP-T-Flower (red) and Flower mutant-mTFP (green) constructs. Bar, 5 µm. **(D)** SIM images of SybKI CTLs (control) and Flower KO/SybKI CTLs in contact with target cells with endocytic anti-RFP647 (magenta). CTLs were incubated with target cells for 30 min in the presence of anti-RFP647 to visualize endocytic CGs. Flower KO/SybKI CTLs were transfected with Flower(WT)-mTFP and Flower(mut)-mTFP separately (bottom two rows) to observe the rescue. Bars, 5 µm. **(E)** Quantitative analysis from panel D of endocytic anti-RFP647 fluorescence signal at the IS. Data are given as mean ± SEM; unpaired Student's t test: ***, $P < 0.001$.

pLysS as outlined in Fig. S1. The full-length 171 amino acid mouse Flower was recovered and purified after cleavage of the fusion protein by His-tagged SUMO-protease Ulp1 (Fig. S1). Two rabbits were injected with the recombinant protein (200 µg each per injection) seven times at 2-wk intervals; bleedings taken after the fourth to seventh immunizations were tested for the presence of anti-Flower antibodies by Western blots of Cos-7 cell lysates, nontransfected or transfected with the mFlower cDNA. Antibodies were affinity-purified from serum on immobilized recombinant mFlower protein. To increase specificity the affinity-purified anti-Flower antibody, it was preabsorbed at spleen homogenates prepared from $mFl^{-/-}$ mice before use.

Experimental models

Procedures involving mice strictly followed National Institutes of Health guidelines and were approved by the Institutional Animal Care and Use Committees at Saarland University and Saarland, Germany. Mice were maintained in a pathogen-free facility under standard housing conditions with continuous access to food and water. Mice used in the study were 2–8 mo old and were maintained on a diurnal 12-h light/dark cycle. Mice did not display obvious health abnormalities and were not subject to prior procedures. The genotype of mice is described where appropriate. The Flower KO mice ($mFl^{-/-}$) were generated by homologous recombination deleting the complete protein-coding exons 2 and 3. The Synaptobrevin2-mRFP knock-in mouse has been described (Matti et al., 2013). Homozygous Synaptobrevin2-mRFP knock-in/Flower KO mice ($mFl^{-/-}/SybKI_{homozygous}$) were generated by crossing homozygous Synaptobrevin2-mRFP knock-in males with $mFl^{-/-}$ females. Mice heterozygous for both loci were subsequently mated to get double-homozygous mice.

Generation of mFlower-deficient mice

To generate mFl-deficient mouse lines, a targeting construct (HTG RS6009_A_G03; Eucomm) was obtained, sequenced on both strands, and introduced into the mFl gene locus of C57BL6 ES cells by gene targeting (Fig. S2). After selection with neomycin, 257 ES cell clones were isolated (by the ingenious targeting laboratory) and analyzed with

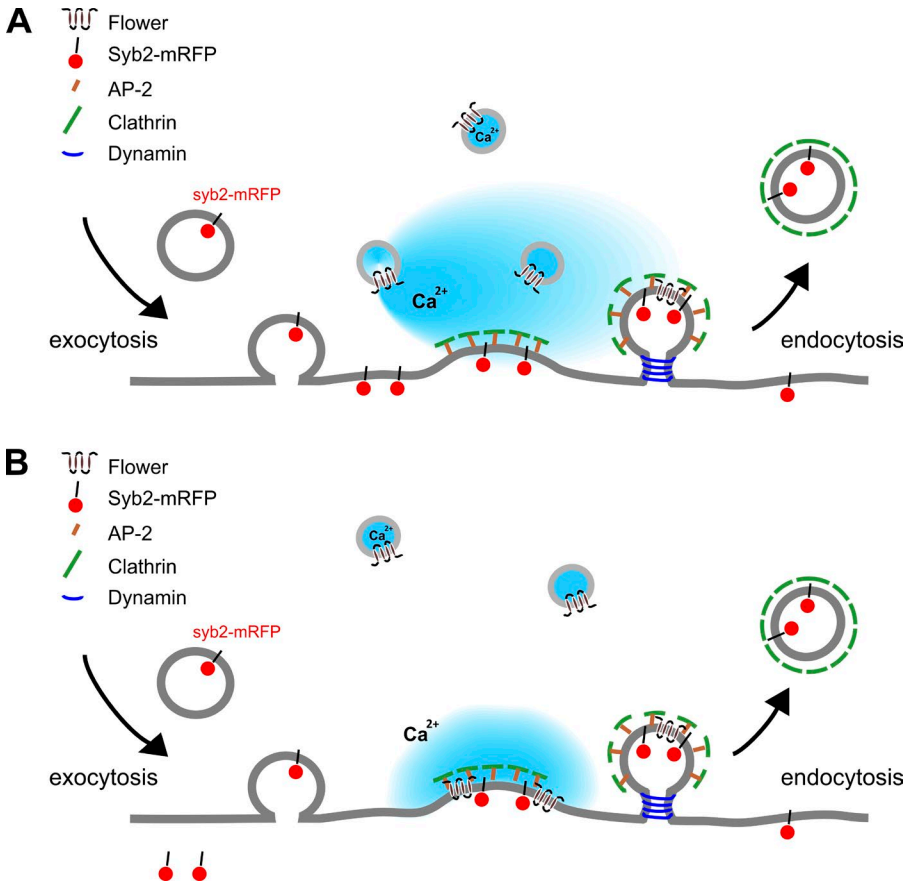

Figure 9. **Alternative models for Flower function in CG endocytosis. (A)** Flower resides on intracellular vesicles and acts as a calcium channel. Flower-mediated efflux from these vesicles triggers endocytosis of CGs. **(B)** Flower-containing vesicles fuse with the plasma membrane at the IS. Flower in the plasma membrane recruits endocytic adaptor proteins such as AP-2 in a calcium-dependent manner to trigger endocytosis of CGs.

Southern blot by using a 3′probe, and 229 turned out to be positive. Two of them, positive for 5′probe and neomycin resistance gene (neo) probe (Fig. S2 B) were selected for injection into BalbC blastocysts, and one of them (clone 1.2D3) created highly chimeric offspring showing germline transmission after breeding with C57BL6/N WT animals, producing pups heterozygous for the L3F2 allele. The L3F2 allele contains a gene cassette (splice acceptor [SA] site–internal ribosomal entry site [IRES]–β-galactosidase cDNA [βGal]–polyadenylation signal-neo) inserted after exon 1 of the mFl gene, comprising the SA site followed by an IRES, a βGal, a polyadenylation signal, and a neo. The gene cassette is flanked by consensus recombination sites of Flp recombinase (FRT sites). In addition, the construct contains loxP sites after the βGal cassette and flanking exons 2 and 3. On Flp recombinase-mediated recombination the SA-IRES-βGal-neo cassette is removed and subsequent Cre recombinase-mediated recombination generates the KO allele (mFl KO; Fig. S2 C). After crossing mFl^{L3F2} mice with a Cre-deleter strain, $mFl^{-/-\beta Gal}$ mice were generated (Fig. S2 D). All experiments were performed with *Fl*$^{-/-}$ and *Fl*$^{-/-}$*βGal* mice. Oligodesoxynucleotide primers used for genotyping are indicated in Table S4. Absence of mFl proteins was confirmed by using Western blot analysis.

Cell culture

Splenocytes were isolated from 8–10-wk-old Synaptobrevin2-mRFP knock-in (SybKI), Flower KO, SybKI crossbred Flower KO (Flower KO/SybKI), or C57BL6/N (WT) mice as described before (Dudenhöffer-Pfeifer et al., 2013). In brief, naive CD8 T cells were positively isolated from splenocytes by using Dynabeads FlowComp Mouse CD8 kit (Invitrogen) as described by the manufacturer. The isolated naive CD8 T cells were cultured for 3 d at 37°C with 5% CO_2. Cell were stimulated with anti-CD3/anti-CD28 activator beads (1:0.8 ratio) at a density of 10^6 cells/ml in Iscove's Modified Dulbecco's Medium (Invitrogen) containing 10% FCS, 0.5% pen/strep (Invitrogen), and 50 µM 2-mercaptoethanol (Roth) to generate effector CTLs. P815 target cells were cultured in RPMI medium (Invitrogen) containing 10% FCS, 1% pen/strep (Invitrogen), and 10 mM Hepes (Invitrogen).

Western blot

Lysates of whole-brain tissue, naive, and 3-d stimulated CTLs isolated from WT and Flower-deficient mice were used to detect Flower expression by using the anti-flower antibody. For preparing lysates, whole-brain tissue was mechanically sheared by using a glass rod in glass homogenizers, whereas cell lysate was homogenized by using a syringe in lysis buffer containing 50 mM Tris-Cl, pH 7.4, 1 mM EDTA, 250 µM PMSF, 1% Triton X-100, 150 mM NaCl, 1 mM DTT, 1 mM deoxycholate, and protease inhibitors (Roche) on ice. Lysates were rotated for 30 min at 4°C. The insoluble materials in lysates were pelleted down by centrifugation at 16,000 *g* for 10 min. The supernatants were the lysate for Western blot. The protein concentration was determined by Bradford assay (Thermo Fisher Scientific). 20-µg lysates were loaded onto 4–12% SDS-PAGE gels (NuPAGE; Invitrogen) to separate proteins. Proteins were then transferred to nitrocellulose membrane and blocked with 5% nonfat milk in TBS buffer containing 20 mM Tris, 0.15 M NaCl, and 0.05% Tween 20, pH 7.4, for 2 h at RT. The membrane was blotted with anti-Flower antibody (1:1,000) for 2 h at RT. Finally, the blot was developed by using enhanced chemiluminescence reagents (SuperSignal West Dura Chemiluminescent Substrate; Thermo Fisher Scientific) and imaged by gel documentation (FluorChem E system; BioLabTec GbR).

Degranulation assay

For the degranulation assay, naive cells were cultured for 3 d with anti-CD3/anti-CD28 beads in a cell/bead ratio of 1:0.4 to stimulate cells.

Stimulated cells (0.2×10^6) were rested for 2 h by removing beads from culture before the assay. Cells were incubated in anti-CD3- (for stimulated cells) or PBS- (for constitutive cells) coated 96-well plates with 0.1 µl anti-CD107a-PE along with 0.15 µl Golgi-stop containing monensin to block intracellular protein transport for 3 h at 37°C for degranulation. Control cells were incubated in PBS-coated wells without anti-CD107a-PE and Golgi-stop as a background signal for FACS analysis. Cells were then washed twice with ice-cold PBS containing 0.5% BSA and analyzed by using the FACS CantoII analyzer (BD PharMingen). Data were analyzed using FlowJo software (Celeza). Gates were set based on nonfluorescent control cells. Each of the individual experiments was done in triplicate and two independent experiments are shown.

Real-time calcein release-based killing assay

P815 cells were loaded with calcein-AM (500 nM; Life Technology) in Roswell Park Memorial Institute medium with 10 mM Hepes for 15 min at RT, washed once, and plated into 96-well black plates with clear bottoms (BD Falcon). Triton X-100 (1%) was added to the target cells to calculate maximal target cell lysis as the control. WT and Flower-deficient CTLs were added with different ratios to settled target cells (2.5×10^4 cells per well) to measure killing at 37°C. Killing was measured every 10 min for 4 h. Reading was performed at 485 nm excitation wavelength and 535 nm emission wavelength in the bottom reading mode by a GENios Pro plate reader. The fluorescence for the experimental conditions was adjusted by the parameter γ according to the live target cell control fluorescence. The γ value was measured at time zero: $\gamma = F_{live}(0)/F_{exp}(0)$. The cytotoxicity was calculated according to the loss of calcein fluorescence in target cells by using the following equation: % target cell lysis $= (F_{live} - \gamma \times F_{exp})/(F_{live} - F_{lyse}) \times 100$, where F_{live} is the fluorescence of only target cell controls, F_{exp} are the CTLs with target cells, and F_{lyse} is the maximal target lysis. The details of this calcein-based killing assay were described previously (Kummerow et al., 2014). All experiments were performed as duplicates and averaged to obtain one dataset.

Confocal live-cell imaging

WT and Flower KO CTLs were transfected with syb2-mRFP plasmid as a CG marker for imaging experiments. CTLs (0.1×10^6) were settled on glass coverslips coated with 0.1 mg/ml poly-L-ornithine for 3 min. 0.02×10^6 cells target cells were added to the coverslip followed by addition of 50 µg/ml anti-CD3e antibody and 30 µg/ml anti-RFP488 antibodies to the coverslip for visualizing CG endocytosis. For the calcium rescue experiment shown in Fig. 5, syb2-mRFP transfected CTLs were imaged with target cells for 7.5 min and then perfused with extracellular buffer containing 2 mM Hepes, 140 mM NaCl, 4.5 mM KCl, 2 mM $MgCl_2$, and 10 mM $CaCl_2$. All experiments were performed at 37°C with 5% CO_2 on the stage of an inverted microscope (LSM 780; Carl Zeiss Microscopy GmbH). Images were acquired with a 40× plan-Apochromat objective (1.3 NA) by using Zen2012 software (Carl Zeiss Microscopy GmbH). The analysis of CG endocytosis shown in Figs. 3 B and 5 B was done by calculating the percentage of total fluorescence of the anti-RFP488 antibody at the IS (fluorescence at the IS/fluorescence in the entire cell × 100) over time. The CTL was divided into three equal parts in volume, and the IS was defined as one third of the CTL (area) facing the target cell. For Fig. 7 A, Flower-deficient CTLs were cotransfected with Flower-pHluorin and syb2-mRFP plasmids to image the dynamics of Flower, CGs, and the endocytic CGs. The transfected CTLs were incubated with target cells in the presence of anti-RFP405 antibody to label endocytosed CGs. The image acquisition was in six steps at 1-µm interval distance for each image and ∼1-s scanning speed. Images are shown as maximal-intensity projection spanning a total thickness of 5 µm. No manipulations except adjustment for brightness was applied to the images. Analyses were done in ImageJ (https://imagej.nih.gov).

Immunofluorescence and SIM

CTLs were stained with anti-Flower antibody to detect endogenous Flower expression in WT and Flower-deficient cells as well as costaining with anti-HA antibody to test the specificity of flower antibody. Cells were fixed in freshly prepared, ice-cold 4% PFA in D-PBS (Invitrogen) washed thrice with PBS and permeabilized for 1 min in D-PBS containing 0.1% Triton X-100 (Roth) and then blocked for 30 min in blocking buffer (D-PBS containing 0.1% Triton X-100 and 5% BSA) for immunostaining. Cells were stained with primary anti-Flower (1:100) or anti-HA (1:500) antibodies, anti–rabbit secondary antibodies (1:1,000) and then mounted for imaging. For the experiment comparing the localization of Flower to endosomal compartments (Fig. 6), stimulated CTLs were transfected with rab5-mCherry, rab7-mCherry, or rab11-mCherry as early, late, or recycling endosome markers, respectively. SybKI CTLs were used as an "endogenous" CG marker. CTLs were then stained with anti-Flower antibody to analyze the colocalization of flower to these compartments by Manders' overlap coefficient (Manders et al., 1993). Cells were imaged using high-resolution SIM. The SIM setup used was from Zeiss (ELYRA PS.1; Carl Zeiss Microscopy GmbH). Images were acquired by using Zen2012 software (Carl Zeiss Microscopy GmbH) and a 63× Plan-Apochromat (NA 1.4) objective with excitation light of 488-, 561-, and 647-nm wavelengths and then processed for SIM to obtain higher resolutions. Z-stacks of 200-nm step size were used to scan the cells. Zen2012 software (Carl Zeiss Microscopy GmbH) was used for acquisition and processing of the images for higher resolutions.

TIRFM

CTLs from Flower-deficient and WT mice were electroporated with a syb2-mRFP plasmid as a CG marker to image fusion in TIRFM as described before (Matti et al., 2013). The TIRFM setup was from Olympus (Olympus Europa SE and Co KG) and equipped with a solid-state laser 85 YCA emitting at 561 nm (Melles-Griot). CTLs (0.2×10^6 cells) were resuspended in 30 µl of extracellular buffer (2 mM Hepes, 140 mM NaCl, 4.5 mM KCl, and 2 mM $MgCl_2$) containing no Ca^{2+} and allowed to settle for 1 min on anti-CD3 antibody (30 µg/ml)–coated coverslips. Cells were then perfused with extracellular buffer containing 2 mM Ca^{2+} for lytic granule fusion (1 mM Ca^{2+} for the experiment presented in Fig. 7, B and C). Cells were imaged for 10 min at 561 nm at RT for CG fusion analysis with an Olympus 100× Plan-Apochomat objective (NA 1.45). The acquisition frequency was 10 Hz, and the exposure time was 100 ms. Images were captured with a QuantEM512SC camera (Photometrics) by using Visiview software (Visitron GmbH). Fusion of CGs was analyzed by using ImageJ with the plugin Time series Analyzer V2 0. Data were not altered during acquisition or analyses. A sudden drop in synaptobrevin2-mRFP fluorescence that was within 300 ms (three acquisition frames) was defined as fusion (Ming et al., 2015). For Fig. 7 B, Flower-deficient CTLs were cotransfected with Flower-pHluorin and syb2-mRFP plasmids to measure the dynamics of Flower and CGs. Flower vesicles and CGs polarized to the IS formed on the anti-CD3 antibody-coated coverslip. The number of vesicles was shown according to the corresponding fluorescence intensity to vesicles. For Fig. 2 F, the CG fusion latency defines the duration from the first CG arrival at IS to the granule fusion. For Fig. 2 G, CTLs were transfected with rab11-mCherry as a recycling endosome marker. The polarization latency analyzed the time interval from the cell attaching to the coverslip with a visible membrane signal in the TIRFM plane to the first granule polarizing to the IS.

Flower topology experiments

For investigating Flower topology, three fusion constructs were generated with ratiometric pH-sensitive pHluorin as a tag, pHluorin fused to the C terminus (Flower-pHluorin), into the loop in between TM2 and TM3 (Flower-loop-pHluorin) of Flower, and as an internal control, pHluorin fused to the C terminus of syb2 (syb2-pHluorin). On acidification of the cytoplasm in the presence of CCCP, the excitation of pHluorin at 395 nm decreases with a corresponding increase in the excitation at 475 nm in both Flower constructs. In brief, stimulated cells were transfected with the cDNAs of Flower-pHluorin, Flower-loop-pHluorin, and syb2-pHluorin individually and 0.2×10^6 cells were settled on a glass coverslip for 5 min, and fluorescence was recorded before and after perfusing 50 µM CCCP in Hepes-based buffer containing 2 mM Ca at the excitation of 405 and 488 nm at a confocal microscope (LSM 780; Zeiss) by using a 40× objective. To compare the topology of the *Drosophila* Flower to the mouse Flower protein, CTLs were transfected with drFlower cDNA with mRFP fused to the C terminus (drFlower-mRFP). Cells were fixed with 4% PFA on glass coverslips then permeabilized in the absence (control) or presence of 0.1% Triton X-100, incubated with anti-RFP488 for 10 min, and mounted for imaging. Mouse hippocampal neurons were cultured in neurobasal A medium for 7 d at 37°C with 5% CO_2 in a 6-well plate and cotransfected with drFlower-mRFP and mFlower-mTFP by calcium phosphate transfection. Cells were fixed and mounted for imaging 24 h after transfection.

CLEM

In a sample preparation, WT and Flower-deficient CTLs were used for CLEM experiments 3 d after activation by anti-CD3/anti-CD28 beads. 4,000 CTLs were seeded on poly-L-ornithine-coated 1.4-mm sapphire discs in flat specimen carriers (Leica) for 5 min to allow cells to settle down. P815 cells (~4,000) premixed with anti-CD3 and anti-RFP488 antibodies were then added to the sapphire discs and incubated for 35 min at 37°C with 5% CO_2 to generate CTL-target cell contacts. Cells were resuspended into Iscove's Modified Dulbecco's Medium containing 30% FCS to maintain better cell morphology after high-pressure freezing (EM PACT2; Leica). The used antibody concentrations were described above in the Confocal live-cell imaging section. Freeze substitution and embedding in Lowicryl was done as described previously (Matti et al., 2013). In brief, all samples were further processed in an automatic freeze-substitution apparatus (AFS2; Leica). The carriers with the frozen specimens were cryo-transferred into dry, flat embedding molds inside the precooled (−130°C) freeze-substitution chamber of the AFS2. The temperature was increased from −130 to −90°C for 2 h. Cryo-substitution was performed at −90 to −70°C for 20 h in anhydrous acetone and at −70 to −60°C for 20 h with 0.3% (wt/vol) uranyl acetate in anhydrous acetone. At −60°C the samples were infiltrated with increasing concentrations (30, 60, and 100%; 1 h each) of Lowicryl (3:1 K11M/HM20 mixture with 0.3% uranyl acetate). After 5 h of 100% Lowicryl infiltration, samples were UV polymerized at −60°C for 24 h and for an additional 15 h while the temperature was raised linearly to 5°C. Samples were kept in the dark at 4°C until further processing. After removing the sapphire discs, 100-nm ultrathin sections were cut parallel to the surface by using an EM UC7 (Leica). The 100-nm ultrathin sections were collected on carbon-coated 200-mesh copper grids (Plano). Fluorescence analysis of EM grids was performed within 1 d after sectioning to avoid loss of fluorescence signals in the sections.

For fluorescence microscopy and EM, 100-nm resin sections were stained with CellMask deep red (Invitrogen) for 10 min (1/500 in 1×PBS), washed in water for 1 min, and analyzed by fluorescence microscopy before EM. The grids were placed in a drop of water between two coverslips that were sealed with vacuum grease (Kukulski et al., 2011). Sections were imaged with the use of high-resolution SIM. The SIM setup (ELYRA PS.1; Zeiss) was described before (Matti et al., 2013). Images were acquired by using the 63× Plan-Apochromat (NA 1.4) with excitation light of 488- and 642-nm wavelengths and processed. Almost the entire field of view of a 200-mesh grid (around 90 μm^2) could be observed with a 63× oil objective by SIM, allowing a perfect orientation relative to the grid bars. After imaging in the bright-field mode, the CellMask deep red image (642 nm) was recorded to identify both the image plane and perfect contacts between CTLs and target cells. After adjusting the highest and lowest focus planes for z-stack analysis, 3–8 anti-RFP488 images (488 nm) were recorded with a step size of 100 nm to scan the cells of interest. Zen2010 software (Carl Zeiss Microscopy GmbH) was used for data acquisition and processing of images for higher resolution. The very same grids were stained with uranyl acetate and lead citrate and analyzed with a Philips Tecnai12 Biotwin electron microscope. Only CTLs, which formed a tight IS (0- to 500-nm cleft) and showed well-conserved membranes, cell organelles, and nuclei were analyzed and used for correlation.

For correlation, the CellMask deep red image, which stains the membranes and organelles of cells, was used to find the optimal overlay on the EM image. The final alignment with the anti-RFP488 image defines the position of the fluorescent signal within the cells of interest. Images were overlaid in Corel Draw.

Fura-2 AM calcium measurements

CTLs isolated from WT and Flower-deficient mice were cultured and stimulated for 3 d with anti-CD3/anti-CD28 activator beads (see Cell culture). At least 2 h before the experiments, activator beads were removed to obtain resting effector CTLs. For cytosolic Ca^{2+} measurements, cells were shortly spun down, resuspended in external solution A containing 140 mM NaCl, 2.8 mM KCl, 1 mM $CaCl_2$, 2 mM $MgCl_2$, 10 mM Hepes, and 10 mM glucose, and loaded with 2 µM Fura-2-AM (Fura-2-acetoxymethylester; TEFLabs) for 30 min at RT in the dark. After a short centrifugation, CTLs were washed and resuspended in external solution A and pipetted into a bath chamber onto poly-L-ornithine- or anti-CD3-coated coverslips. The microscope was focused onto cells already on top of the coverslip, and fluorescence measurements were started immediately. As soon as farther CTLs settled down, they came into focus, and cytosolic Ca^{2+} changes on touching the poly-L-ornithine- (control) or anti-CD3- (stimulation) coated coverslips were detected. The Ca^{2+}-dependent Fura-2 fluorescence of single CTLs was monitored at a rate of 0.5 Hz with a dual excitation fluorometric imaging system (Polychrome V; TILL Photonics) controlled by TILLvisION software by using a Zeiss Axiovert S100 microscope equipped with a 20× Fluar objective (NA 0.8; Zeiss). Fura-2-loaded cells were excited at 340 nm and 380 nm for 30 ms each, and the fluorescence emission >450 nm was detected by a TILL IMAGO CCD camera. After background subtraction, cells were marked as regions of interest, and their mean fluorescence at 340- (F340) and 380-nm (F380) excitation were computed into relative ratio units (F340/F380) and transferred to IGOR Pro (WaveMetrics) for further analysis and preparation of the figures. To compare and average the cellular responses on touching the poly-ornithine– or anti-CD3–coated coverslips, the time points of touch-down were merged.

Preparation of microsomal membranes and cell lysates for antibody-based affinity enrichment of Flower-containing protein complexes followed by MS

All steps were done on ice and with cold buffers (4°C). Freshly prepared mouse brains were homogenized in lysis buffer (0.1 M Tris-HCl, pH 8.0, 1 mM $MgCl_2$, and protease inhibitor mix, and 100 mg tissue/ml lysis buffer) and homogenized consecutively by polytron and glass-Tef-

lon potter treatment. The homogenate was frozen at −80°C for 20 min, quickly thawed at RT, placed on ice, and sheared 10 times through a needle (diameter = 0.55 mm). The homogenate was then diluted 1:6 by saccharose buffer (0.25 M saccharose and 10 mM Tris-HCl, pH7.4) and centrifuged at 3,000 *g* for 20 min. The supernatant was separated and centrifuged at 100,000 *g* for 40 min. The pellet (microsomal membrane fraction) was resuspended in saccharose buffer and homogenized by a glass-Teflon potter, and aliquots were frozen at −80°C. Protein concentration was determined by BCA assay (Pierce).

Affinity-purified mFl antibodies or nonrelated rabbit immunoglobulins as negative controls were covalently coupled to magnetic M-280 tosyl-activated beads (Invitrogen) as described (Fecher-Trost et al., 2013) or were bound (10 µg affinity-purified mFl antibodies or rabbit IgGs) to 50 µl protein A magnetic beads (NEB) in TBS (150 mM NaCl and 50 mM Tris-HCl, pH 7.4) buffer. To obtain the solubilized protein fractions, 10 mg microsomal proteins prepared from mouse brain or CTLs was resuspended in 20 ml IP buffer (150 mM NaCl, 50 mM Tris-HCl, pH 8.0, 5 mM EDTA, and protease inhibitor cocktail [Roche]) supplemented with 1,25% dodecylmaltosid (brain) or a mixture of 0.1% Triton X-100 and 0.2% dodecylmaltosid (CTLs), homogenized with a glass-Teflon potter, and incubated by shaking for 45 min at 4°C. After centrifugation at 100,000 *g* at 4°C for 45 min, the supernatant was incubated with the antibodies coupled to magnetic beads overnight at 4°C. The beads were collected with a magnetic rack and washed with 1 ml IP buffer six times. Proteins were eluted with 40–60 µl denaturing SDS sample buffer (final concentration: 60 mM Tris-HCl, pH 6.8, 4% SDS, and 10% glycerol including 0.72 M β-mercaptoethanol) at 60°C for 20 min and shortly electrophoresed (∼1 cm, 15 min, 180 V) on NuPAGE (Invitrogen) 4–12% gradient gels, fixed in the presence of 40% ethanol and 10% acetic acid, and visualized with colloidal Coomassie stain (20% [vol/vol] methanol, 10% [vol/vol] phosphoric acid, 10% [wt/vol] ammonium sulfate, and 0.12% [wt/vol] Coomassie G-250). The whole sample was cut into 3–4 gel slices and alternately washed twice with solution A (50 mM NH_4HCO_3) and solution B (50 mM NH_4HCO_3 and 50% [vol/vol] acetonitrile). Reduction of disulfide bridges was obtained by incubation at 56°C for 30 min in 50 mM NH_4HCO_3 and 10 mM dithiothreitol, followed by carbamidomethylation at 20°C in darkness for 30 min in the presence of a solution containing 50 mM NH_4HCO_3 and 5 mM iodoacetamide. Gel pieces were washed twice alternating with solutions A and B and then dried in a vacuum centrifuge. For in-gel digestion, the gel pieces were incubated in the presence of 15–20 µl porcine trypsin (20 ng/µl; Promega) at 37°C overnight. Resulting peptides were extracted twice by shaking the gel pieces in extraction buffer (2.5% formic acid and 50% acetonitrile). Extracted peptides were concentrated in a vacuum centrifuge, resuspended in 22 µl in 0.1% formic acid, centrifuged for 15 min at 10,000 *g*, and 20 µl of the supernatant was transferred to glass vials with inserts (Macherey and Nagel) and sealed. Subsequently, an aliquot of the tryptic peptide extracts for each antibody or IgG control purification was analyzed by online nanoflow LC-HR-MS/MS (Ultimate 3000 RSLC nano system equipped with an Ultimate3000 RS autosampler coupled to an LTQ Orbitrap Velos Pro; all Thermo Fisher Scientific). Peptides were trapped on a C18 trap column (75 µm × 2 cm, Acclaim PepMap100C18, 3 µm; Thermo Fisher Scientific) and separated on a reversed-phase column (nano viper Acclaim PepMap capillary column, C18; 2 µm; 75 µm × 25 cm and 75 µm × 50 cm; Dionex) at a flow rate of 200 nl/min with buffer A (water and 0.1% formic acid) and B (90% acetonitrile and 0.1% formic acid) by using gradient 1 (4 to 55% buffer B in 56 min; 55 to 90% B in 7 min) and gradient 2 (4 to 40% buffer B in 66 min; 40 to 90% B in 20 min). The effluent of the chromatography was directly sprayed into the mass spectrometer through a coated silica electrospray emitter (PicoTipEmitter, 30 µm; New Objective) and ionized at 2.2 kV. MS spectra were acquired in a data-dependent mode (automatic switch between full-scan MS and MS/MS). For the collision-induced dissociation MS/MS top10 method (gradient 1 and 2), full-scan MS spectra (*m/z* 300–1,700) were acquired in the Orbitrap analyzer by using a target value of 10^6 with a resolution of r = 60,000. The 10 most intense peptide ions with charge states >2 were fragmented in the high-pressure linear ion trap by low-energy collision-induced dissociation with normalized collision energy of 35%.

Raw liquid chromatography (LC)–MS data analysis

The fragmented peptides were identified by using MASCOT algorithm and Proteome Discoverer 1.4 software. Peptides were matched to tandem mass spectra by Mascot version 2.4.0 (Matrix Science) by searching the UniProtKB database (version2015_01, number of protein sequences all taxonomies: 547.599, taxonomy mouse:16.706, and a modified UniProtKB database including the protein sequences of Flower-TFP and Flower mutant-TFP). MS^2 spectra were matched with a mass tolerance of 7 ppm for precursor masses and 0.5 D for fragmented ions. We used tryptic digest and allowed for up to two missed cleavage sites. Cysteine carbamidomethylation was set as a fixed modification, and deamidation of asparagine and glutamine, acetylation of lysine, and oxidation of methionine were set as variable modifications. Resulting Dat-files obtained from Mascot were also loaded in Scaffold 4. To obtain the relative or semiquantitative amount of peptides in the mFl and IgG immunoprecipitation samples, we used three independent methods: (1) The peak area calculation quantification in which we used a Proteome Discoverer 1.4 workflow, including the "precursor ion area detection" node (settings: minimal precursor 350 D, maximal precursor 5,000 D, total intensity threshold 1,000). This method calculates the area of a measured protein as the average of the three most abundant distinct peptides identified for this protein (TOP^3 peak area) reported by (Silva et al., 2006). (2) The relative exponentially modified sequence coverage (remSC) value was calculated according to previous studies (Ishihama et al., 2005; Berkefeld et al., 2006) as the ratio of exponentially modified sequence coverages obtained for any given protein from eluates of the anti-mFl or control IgGs. Sequence coverage is the primary protein sequence actually identified by the MS/MS spectra versus the theoretically identifiable primary sequence in MS/MS analyses. (3) The relative peptide query (rPQ) score is the ratio of peptide queries obtained for any given protein from eluates of the anti-mFl antibody and control IgG pools; the peptide query value of a protein is defined as the summation of all Mascot MS/MS spectra (queries). For proteins not detected in the IgG controls, a detection limit of 0.125 (queries) was used as a denominator in the rPQ score. The resulting log rPQ scores for Flower and AP proteins were shown in a diagram with a specificity threshold for log rPQ at a value of 0.6. Accordingly, AP proteins with values for the rPQ score >4 were classified to be specifically purified by the anti-mFl antibodies. The abundance ratio of the TFP-tagged Flower WT and the Flower AP-2–binding mutant (emPAI Flower mutant/emPAI Flower WT) were calculated from the normalized emPAI values (extracted from Scaffold) obtained in the Flower-TFP or Flower mutant-TFP containing protein complexes enriched by the anti-TFP antibody.

Statistics

Data were analyzed by using SigmaPlot Version9. Student's unpaired *t* test, one-sample *t* test, and Mann-Whitney *U* test were used to evaluate significant differences between data.

Online supplemental material

Online supplemental material contains generation of the anti-Flower antibody (Fig. S1), the Flower KO mouse strain (Fig. S2), the experi-

mental evidence for the Flower transmembrane topology (Fig. S3), and identification of AP-2 proteins coassembled with Flower by MS (Fig. S4 and Table S1). Furthermore, all plasmids and antibodies (Tables S2 and S3) as well as oligonucleotides (Table S4) generated and used in this study are listed. In addition, Video 1 shows the specific block of endocytosis in CTLs from Flower-deficient mice by confocal microscopy, Video 2 the 3D reconstruction of WT and Flower-deficient CTLs to demonstrate the block of endocytosis due to Flower deficiency, Video 3 the rescue of the Flower phenotype by elevated calcium (confocal microscopy), and Videos 4 and 5 the polarization of Flower-containing vesicles to the IS before CG polarization (confocal microscopy and TIRFM, respectively).

Acknowledgments

We thank Dr. Petra Weissgerber and the Transgene Unit of the specific pathogen-free animal facility of the Medical Faculty, Homburg, and Stefanie Buchholz, Anja Ludes, Anne Kunkel, and Karin Wolske for excellent technical assistance. We thank Dr. Martin Jung and Sabine Pelvay for immunizing and bleeding rabbits, Dr. Ulrich Wissenbach for help in initial cloning, Dr. Annette Lis for help with the calcein killing assay, and Dr. David Stevens for valuable suggestions.

This project was funded by Deutsche Forschungsgemeinschaft/Sonderforschungsbereich 894.

The authors declare no competing financial interests.

Author contributions: H.-F. Chang conceived and performed imaging experiments. S. Mannebach generated Flower cDNA constructs and Flower KO mice. K. Frohnweiler generated recombinant proteins and antibody. A. Beck performed Fura-2 measurements (and patch-clamp experiments). C. Fecher-Tost performed protein purification and mass spectrometry experiments. K. Ravichandran performed real-time killing assays and FACS analyses. E. Krause helped with FACS analyses, imaging data analyses, and the movies. C. Schirra conceived and performed CLEM experiments. V. Pattu provided expertise and feedback. V. Flockerzi and J. Rettig contributed to all aspects of the manuscript (provided expertise, supervision, and review and wrote and edited the manuscript).

Submitted: 9 June 2017
Revised: 9 November 2017
Accepted: 29 November 2017

References

Beck, K.A., and J.H. Keen. 1991. Interaction of phosphoinositide cycle intermediates with the plasma membrane-associated clathrin assembly protein AP-2. *J. Biol. Chem.* 266:4442–4447.

Berkefeld, H., C.A. Sailer, W. Bildl, V. Rohde, J.O. Thumfart, S. Eble, N. Klugbauer, E. Reisinger, J. Bischofberger, D. Oliver, et al. 2006. BKCa-Cav channel complexes mediate rapid and localized Ca2+-activated K+ signaling. *Science.* 314:615–620. https://doi.org/10.1126/science.1132915

Brose, N., and E. Neher. 2009. Flowers for synaptic endocytosis. *Cell.* 138:836–837. https://doi.org/10.1016/j.cell.2009.08.023

Chang, H.F., H. Bzeih, C. Schirra, P. Chitirala, M. Halimani, E. Cordat, E. Krause, J. Rettig, and V. Pattu. 2016. Endocytosis of cytotoxic granules is essential for multiple killing of target cells by T lymphocytes. *J. Immunol.* 197:2473–2484. https://doi.org/10.4049/jimmunol.1600828

Dudenhöffer-Pfeifer, M., C. Schirra, V. Pattu, M. Halimani, M. Maier-Peuschel, M.R. Marshall, U. Matti, U. Becherer, J. Dirks, M. Jung, et al. 2013. Different Munc13 isoforms function as priming factors in lytic granule release from murine cytotoxic T lymphocytes. *Traffic.* 14:798–809. https://doi.org/10.1111/tra.12074

Fecher-Trost, C., U. Wissenbach, A. Beck, P. Schalkowsky, C. Stoerger, J. Doerr, A. Dembek, M. Simon-Thomas, A. Weber, P. Wollenberg, et al. 2013. The in vivo TRPV6 protein starts at a non-AUG triplet, decoded as methionine, upstream of canonical initiation at AUG. *J. Biol. Chem.* 288:16629–16644. https://doi.org/10.1074/jbc.M113.469726

Gad, H., P. Löw, E. Zotova, L. Brodin, and O. Shupliakov. 1998. Dissociation between Ca2+-triggered synaptic vesicle exocytosis and clathrin-mediated endocytosis at a central synapse. *Neuron.* 21:607–616. https://doi.org/10.1016/S0896-6273(00)80570-X

Gogna, R., K. Shee, and E. Moreno. 2015. Cell competition during growth and regeneration. *Annu. Rev. Genet.* 49:697–718. https://doi.org/10.1146/annurev-genet-112414-055214

Griffiths, G.M., A. Tsun, and J.C. Stinchcombe. 2010. The immunological synapse: A focal point for endocytosis and exocytosis. *J. Cell Biol.* 189:399–406. https://doi.org/10.1083/jcb.201002027

Hogan, P.G., R.S. Lewis, and A. Rao. 2010. Molecular basis of calcium signaling in lymphocytes: STIM and ORAI. *Annu. Rev. Immunol.* 28:491–533. https://doi.org/10.1146/annurev.immunol.021908.132550

Ishihama, Y., Y. Oda, T. Tabata, T. Sato, T. Nagasu, J. Rappsilber, and M. Mann. 2005. Exponentially modified protein abundance index (emPAI) for estimation of absolute protein amount in proteomics by the number of sequenced peptides per protein. *Mol. Cell. Proteomics.* 4:1265–1272. https://doi.org/10.1074/mcp.M500061-MCP200

Klingauf, J., E.T. Kavalali, and R.W. Tsien. 1998. Kinetics and regulation of fast endocytosis at hippocampal synapses. *Nature.* 394:581–585. https://doi.org/10.1038/29079

Kukulski, W., M. Schorb, S. Welsch, A. Picco, M. Kaksonen, and J.A. Briggs. 2011. Correlated fluorescence and 3D electron microscopy with high sensitivity and spatial precision. *J. Cell Biol.* 192:111–119. https://doi.org/10.1083/jcb.201009037

Kummerow, C., E.C. Schwarz, B. Bufe, F. Zufall, M. Hoth, and B. Qu. 2014. A simple, economic, time-resolved killing assay. *Eur. J. Immunol.* 44:1870–1872. https://doi.org/10.1002/eji.201444518

Kuo, S.P., and L.O. Trussell. 2009. A new ion channel blooms at the synapse. *Neuron.* 63:566–567. https://doi.org/10.1016/j.neuron.2009.08.031

Lancki, D.W., A. Weiss, and F.W. Fitch. 1987. Requirements for triggering of lysis by cytolytic T lymphocyte clones. *J. Immunol.* 138:3646–3653.

Leibson, P.J., D.E. Midthun, K.P. Windebank, and R.T. Abraham. 1990. Transmembrane signaling during natural killer cell-mediated cytotoxicity. Regulation by protein kinase C activation. *J. Immunol.* 145:1498–1504.

Mahaffey, D.T., J.S. Peeler, F.M. Brodsky, and R.G. Anderson. 1990. Clathrin-coated pits contain an integral membrane protein that binds the AP-2 subunit with high affinity. *J. Biol. Chem.* 265:16514–16520.

Manders, E.M.M., F.J. Verbeek, and J.A. Aten. 1993. Measurement of co-localization of objects in dual-color confocal images. *J Microsc.* 169:375–382. https://doi.org/10.1111/j.1365-2818.1993.tb03313.x

Marshall, M.R., V. Pattu, M. Halimani, M. Maier-Peuschel, M.L. Müller, U. Becherer, W. Hong, M. Hoth, T. Tschernig, Y.T. Bryceson, and J. Rettig. 2015. VAMP8-dependent fusion of recycling endosomes with the plasma membrane facilitates T lymphocyte cytotoxicity. *J. Cell Biol.* 210:135–151. https://doi.org/10.1083/jcb.201411093

Matsui, W., and T. Kirchhausen. 1990. Stabilization of clathrin coats by the core of the clathrin-associated protein complex AP-2. *Biochemistry.* 29:10791–10798. https://doi.org/10.1021/bi00500a011

Matti, U., V. Pattu, M. Halimani, C. Schirra, E. Krause, Y. Liu, L. Weins, H.F. Chang, R. Guzman, J. Olausson, et al. 2013. Synaptobrevin2 is the v-SNARE required for cytotoxic T-lymphocyte lytic granule fusion. *Nat. Commun.* 4:1439. https://doi.org/10.1038/ncomms2467

Merino, M.M., C. Rhiner, M. Portela, and E. Moreno. 2013. "Fitness fingerprints" mediate physiological culling of unwanted neurons in Drosophila. *Curr. Biol.* 23:1300–1309. https://doi.org/10.1016/j.cub.2013.05.053

Ming, M., C. Schirra, U. Becherer, D.R. Stevens, and J. Rettig. 2015. Behavior and properties of mature lytic granules at the immunological synapse of human cytotoxic T lymphocytes. *PLoS One.* 10:e0135994. https://doi.org/10.1371/journal.pone.0135994

Pattu, V., B. Qu, M. Marshall, U. Becherer, C. Junker, U. Matti, E.C. Schwarz, E. Krause, M. Hoth, and J. Rettig. 2011. Syntaxin7 is required for lytic granule release from cytotoxic T lymphocytes. *Traffic.* 12:890–901. https://doi.org/10.1111/j.1600-0854.2011.01193.x

Pichaud, F. 2013. Neuron survival: Say it with Flowers. *Curr. Biol.* 23:R613–R615. https://doi.org/10.1016/j.cub.2013.06.036

Rhiner, C., J.M. López-Gay, D. Soldini, S. Casas-Tinto, F.A. Martín, L. Lombardía, and E. Moreno. 2010. Flower forms an extracellular code that reveals the fitness of a cell to its neighbors in Drosophila. *Dev. Cell.* 18:985–998. https://doi.org/10.1016/j.devcel.2010.05.010

Sankaranarayanan, S., and T.A. Ryan. 2001. Calcium accelerates endocytosis of vSNAREs at hippocampal synapses. *Nat. Neurosci.* 4:129–136. https://doi.org/10.1038/83949

Silva, J.C., M.V. Gorenstein, G.Z. Li, J.P. Vissers, and S.J. Geromanos. 2006. Absolute quantification of proteins by LCMSE: A virtue of parallel MS acquisition. *Mol. Cell. Proteomics.* 5:144–156. https://doi.org/10.1074/mcp.M500230-MCP200

Takayama, H., and M.V. Sitkovsky. 1987. Antigen receptor-regulated exocytosis in cytotoxic T lymphocytes. *J. Exp. Med.* 166:725–743. https://doi.org/10.1084/jem.166.3.725

Xue, L., Z. Zhang, B.D. McNeil, F. Luo, X.S. Wu, J. Sheng, W. Shin, and L.G. Wu. 2012. Voltage-dependent calcium channels at the plasma membrane, but not vesicular channels, couple exocytosis to endocytosis. *Cell Reports.* 1:632–638. https://doi.org/10.1016/j.celrep.2012.04.011

Yao, C.K., Y.Q. Lin, C.V. Ly, T. Ohyama, C.M. Haueter, V.Y. Moiseenkova-Bell, T.G. Wensel, and H.J. Bellen. 2009. A synaptic vesicle-associated Ca2+ channel promotes endocytosis and couples exocytosis to endocytosis. *Cell.* 138:947–960. https://doi.org/10.1016/j.cell.2009.06.033

Yao, C.K., Y.T. Liu, I.C. Lee, Y.T. Wang, and P.Y. Wu. 2017. A Ca2+ channel differentially regulates Clathrin-mediated and activity-dependent bulk endocytosis. *PLoS Biol.* 15:e2000931. https://doi.org/10.1371/journal.pbio.2000931